USGS
science for a changing world

Prepared in cooperation with the U.S. Army Corps of Engineers Kansas City District

Integrated Geophysical Investigation of Preferential Flow Paths at the Former Tyson Valley Powder Farm near Eureka, Missouri, May 2006

Scientific Investigations Report 2008–5212

U.S. Department of the Interior
U.S. Geological Survey

FRONT COVER:

View to the east showing the DC resistivity equipment set up along Line 2 in the floodplain of the former Tyson Valley Powder Farm. Photograph by Bethany L. Burton.

Integrated Geophysical Investigation of Preferential Flow Paths at the Former Tyson Valley Powder Farm near Eureka, Missouri, May 2006

By Bethany L. Burton, Lyndsay B. Ball, Gregory P. Stanton,
and Christopher M. Hobza

Prepared in cooperation with the U.S. Army Corps of Engineers Kansas City District

Scientific Investigations Report 2008–5212

U.S. Department of the Interior
U.S. Geological Survey

U.S. Department of the Interior
DIRK KEMPTHORNE, Secretary

U.S. Geological Survey
Suzette M. Kimball, Acting Director

U.S. Geological Survey, Reston, Virginia: 2009

For product and ordering information:
World Wide Web: http://www.usgs.gov/pubprod
Telephone: 1-888-ASK-USGS

For more information on the USGS—the Federal source for science about the Earth, its natural and living resources, natural hazards, and the environment:
World Wide Web: http://www.usgs.gov
Telephone: 1-888-ASK-USGS

Suggested citation:
Burton, B.L., Ball, L.B., Stanton, G.P., and Hobza, C.M., 2009, Integrated geophysical investigation of preferential flow paths at the former Tyson Valley Powder Farm near Eureka, Missouri, May 2006: U.S. Geological Survey Scientific Investigations Report 2008–5212, 44 p.

Contents

Figures

Tables

Conversion Factors

SI to Inch/Pound

Multiply	By	To obtain
	Length	
centimeter (cm)	0.3937	inch (in.)
meter (m)	3.281	foot (ft)
kilometer (km)	0.6214	mile (mi)
meter (m)	1.094	yard (yd)
	Area	
hectare (ha)	2.471	acre
hectare (ha)	0.003861	square mile (mi^2)
	Flow rate	
cubic meter per second (m^3/s)	70.07	acre-foot per day (acre-ft/d)
meter per second (m/s)	3.281	foot per second (ft/s)
cubic meter per second (m^3/s)	35.31	cubic foot per second (ft^3/s)
cubic meter per second (m^3/s)	22.83	million gallons per day (Mgal/d)
	Mass	
kilogram (kg)	2.205	pound avoirdupois (lb)

Vertical coordinate information is referenced to North American Vertical Datum of 1988 (NAVD 88).

Horizontal coordinate information is referenced to the North American Datum of 1983 (NAD 83).

Elevation, as used in this report, refers to distance above the vertical datum.

Specific conductance is given in microsiemens per centimeter at 25 degrees Celsius (µS/cm at 25°C).

Concentrations of chemical constituents in water are given in micrograms per liter (µg/L)

Integrated Geophysical Investigation of Preferential Flow Paths at the Former Tyson Valley Powder Farm near Eureka, Missouri, May 2006

By Bethany L. Burton, Lyndsay B. Ball, Gregory P. Stanton, and Christopher M. Hobza

Abstract

In May 2006, the U.S. Geological Survey, in cooperation with the U.S. Army Corps of Engineers, conducted surface and borehole geophysical surveys at the former Tyson Valley Powder Farm near Eureka, Mo., to identify preferential pathways for potential contaminant transport along the bedrock surface and into dissolution-enhanced fractures. The Tyson Valley Powder Farm was formerly used as a munitions storage and disposal facility in the 1940s and 1950s, and the site at which the surveys were performed was a disposal area for munitions and waste solvents such as trichloroethylene and dichloroethylene. Direct-current resistivity and seismic refraction data were acquired on the surface; gamma, electromagnetic induction, and full waveform sonic logs were acquired in accessible boreholes. Through the combined interpretation of the seismic refraction tomographic and resistivity inversion results and borehole logs, inconsistencies in the bedrock surface were identified that may provide horizontal preferential flow paths for dense nonaqueous phase liquid contaminants. These results, interpreted and displayed in georeferenced three-dimensional space, should help to establish more effective monitoring and remediation strategies.

Introduction

The former Tyson Valley Powder Farm (TVPF) was owned and operated by the U.S. Army from 1941 to 1947 and again from 1951 to 1961. The former TVPF was used primarily as a storage facility for the production of small arms ammunition, although munitions testing and disposal took place on the site as well (Kring and Bailey, 2001). Area of Concern 2 (AOC 2), also referred to as the Burning Pan Site, was formerly used for incineration of out-of-specification propellants and other flammables. The source area is suspected of containing contamination from fuels, waste oil, and flammable chemicals that were used to incinerate material in the burning pans, as well as contamination from metal and explosive residues resulting from incineration (MicroPact, 2004). In particular, some monitoring wells indicate the dense non-aqueous phase liquid (DNAPL) contaminants trichloroethylene (TCE) and dichloroethylene (DCE) at levels exceeding their maximum contaminant levels (MCLs), which are established by the U.S. Environmental Protection Agency (EPA).

Since DNAPL contaminants are denser than water, they are gravity-driven and can migrate vertically below the water table and flow along hydrologic discontinuities such as a bedrock surface. Observations made during drilling activities at the former TVPF suggest that dissolution zones and fractures may exist in the limestone bedrock that underlies the area. The size, trend, and extent of these features, however, are unknown (David Back, MicroPact, oral commun., March 2006). Fractures and dissolution zones, as well as depressions in the bedrock surface, can create conduits for ground-water flow, leading to preferential flow paths for contaminant transport. To ensure proper monitoring of ground-water contamination, a detailed understanding of localized ground-water movement is imperative. Understanding the occurrence and trend of possible preferential flow paths will lead to a more accurate and efficient remediation plan.

A conventional bedrock mapping study would collect information through drilling test holes. However, test holes only provide data at a single location and test holes are frequently drilled too far apart to adequately characterize localized features of the bedrock surface, such as fractured zones or depressions that may control local ground-water movement. In contrast, surface geophysical methods facilitate the collection of more continuous subsurface geologic information.

Geophysical methods provide information about the spatial distribution of subsurface physical properties, such as electrical conductivity (or its reciprocal, resistivity), dielectric permittivity, magnetic permeability, and energy propagation velocities. There must be sufficient contrast in the physical properties of the subsurface in order for geophysical methods to successfully identify features. For example, the increase in secondary porosity created by fracture networks will result in an increase in water content under saturated conditions. This increase in water content will usually result in a decrease in electrical resistivity when compared to the surrounding unfractured bedrock. Similarly, this fracturing may reduce the competency of the bedrock, reducing its ability to effectively propagate sound waves that would result in a lower velocity than the surrounding rock. These physical contrasts, however, can be the result of many different geologic transitions, resulting in non-unique interpretations. By integrating results from multiple geophysical techniques and comparing these results to lithologic data from existing boreholes, a more realistic geologic interpretation can be achieved.

Purpose and Scope

In May 2006, the U.S. Geological Survey (USGS), in cooperation with the U.S. Army Corps of Engineers (USACE), used integrated borehole and surface geophysical techniques to attempt to characterize localized ground-water movement between AOC 2 and the Meramec River. Specifically, we collected fluid resistivity, electromagnetic induction, gamma, and full-waveform sonic logs in several monitoring wells. We collected direct-current (DC) resistivity and compressional (P-) wave seismic refraction data along six two-dimensional (2D) lines down-gradient from AOC 2. By measuring different physical properties at the same location, method-specific ambiguities were minimized, thereby allowing a more comprehensive and geologically realistic interpretation of the subsurface. Several possible flow paths and fracture zones were identified through this integrated approach.

Study Area Description

The former TVPF site is located in St. Louis County, Mo., approximately 32 km southwest of the city of St. Louis and 5 km northeast of the city of Eureka, Mo. (fig. 1). The former TVPF occupied approximately 1,060 hectares and is currently divided into three areas: Tyson Research Center (TRC), Lone Elk County Park, and West Tyson County Park (Kring and Bailey, 2001). The AOC 2 study area is located near the northeastern boundary of the current Tyson Research Center.

The geophysical study area comprises two settings: the topographically higher upland site near the contaminant source area and the topographically lower floodplain of the Meramec River site to the north. The upland land surface generally slopes downward toward the Meramec River to the north through a series of terraces until crossing the Burlington Northern Santa Fe Railway, where the topography flattens out in the floodplain. Vegetation on the upland site consists of forested areas with a brushy, dense understory except where maintained as mowed grass. The floodplain is a combination of a well-defined forested area with an open understory and a tall grass field closer to the river (fig. 1).

Hydrogeology

Located within the Ozark Plateau physiographic province (Imes and Emmett, 1994), the local surface geology consists of nearly flat lying sedimentary rocks. Tectonic activity that created the Ozark Dome lifted the sedimentary rocks, creating faults and fractures in the Precambrian basement (Imes and Emmett, 1994). As a result, the local bedrock, consisting of multiple middle-Ordovician limestone units (Kimmswick, Decorah, and Plattin Limestones in order of increasing age), dips approximately one degree to the northeast. These sedimentary sequences have been incised by streams to form dendritic drainage patterns and rolling hills. Karst features such as springs, sinkholes, losing streams, caves, and conduits are present in the former TVPF.

The Kimmswick Limestone is 20–34 m thick, occurs as a cliff former, and is karstic in places (Criss, 2001). Underlying the Kimmswick Limestone, the Decorah Group is 8 m thick and is composed of interbedded greenish-gray shales and limestones. Underlying the Decorah Group, the Plattin Limestone is 30 m thick and is composed of gray medium to massive limestone that also has a tendency to form karst features.

The bedrock in the study area is mantled by Quaternary alluvium and regolith. The upland site, in particular, consists of 8–12 m of clay-rich regolith overlying limestone bedrock, which has varying thicknesses of weathered and fractured sections (MicroPact, 2006). The dominant upland soil types are the Menfro silt loam and the Clarksville cherty silt loam (Benham, 1982). The nearby Meramec River Valley contains unconsolidated alluvial deposits of gravel and sand that are 12–18 m thick. These deposits compose a shallow aquifer used by the nearby communities downstream from the TVPF (Criss, 2001). The dominant soil types in the Meramec River floodplain are the Haymond silt loam and the Sarpy loamy fine sand. Both of these alluvial soils are well drained (Benham, 1982).

The mean annual rainfall from 1977 to 2006 at the Tyson Research Center was 108.76 cm with a range of 65.89 (1989) to 148.44 (1981) cm (Larson, 2007). Based on 88 years of data (from 1903 to 2007) from USGS gaging station #07019000 on the Meramec River near Eureka, Mo., the mean daily discharge of the Meramec River is 77 m^3/s with a minimum rate in 1936 of 5.6 m^3/s and a maximum rate in 1982 of 3,900 m^3/s (U.S. Geological Survey, 2007).

Methods

Borehole Geophysical Methods

For this study, we acquired fluid resistivity and temperature, electromagnetic (EM) induction, natural gamma, and acoustic velocity logs in accessible monitoring wells located in AOC 2. All geophysical probes interfaced to a Mount

Figure 1. Aerial photograph of the former TVPF showing the locations of the current Tyson Research Center, the Area of Concern 2 source area (yellow square), the upland study site (red outline), the floodplain study site (green outline), and Castlewood State Park (modified from Ball and others, 2004).

Sopris (Mount Sopris Instrument Company, Inc., Golden, Colo.) MGXII log-acquisition system by way of 0.635-cm-diameter single-conductor wireline.

These tools were chosen based on their potential to help with the interpretation of the surface geophysical data, to map the limestone bedrock topography, and to possibly identify fracture zones within the limestone. The EM induction and sonic logs were used to determine formation resistivity and P-wave velocities, respectively. The gamma log was chosen to determine relative clay and shale content of the subsurface; this log is important for delineating the more conductive zones observed in either the EM induction logs or surface DC resistivity profiles as either water-filled fracture zones or clay- or shale-rich layers. Geophysical logs were run in monitoring wells 21, 23, 27, 29, 33, 34, and 35 (fig. 2). It was discovered at the time of logging in May 2006, however, that all but two of the monitoring wells' construction likely included steel casing, which was not indicated in the construction reports. Monitoring wells 34 (MW34) and 35 (MW35) were the only wells that provided useful, continuous resistivity data. Because of multiple casing strings in other wells, useful sonic data were also limited to MW34 and MW35. Monitoring well 36 (MW36), MW37, and MW38 were drilled after the geophysical field effort and consequently were not logged (fig. 2). All geophysical borehole logs that we acquired are presented in appendix 1.

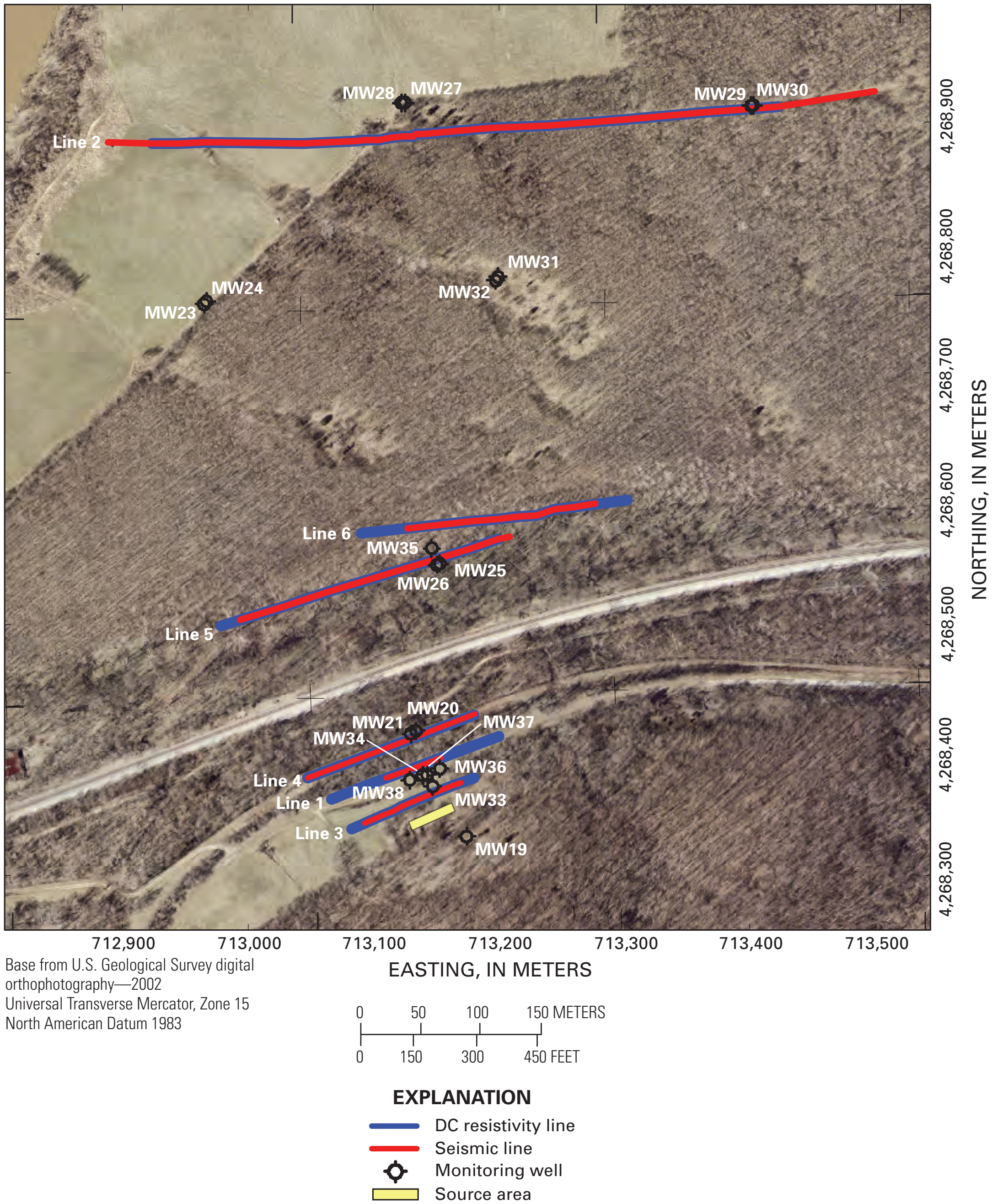

Figure 2. Aerial photograph of the upland and floodplain sites of AOC 2 of the former TVPF showing the locations of the six direct-current resistivity (blue) and seismic refraction (red) lines, nearby monitoring wells, and the approximate source area (yellow rectangle).

Fluid Resistivity and Temperature Logs

Fluid resistivity logs, which provide a record of the capacity of the borehole fluid to conduct electrical current (Keys, 1990), are collected concurrently with fluid temperature. Changes of fluid resistivity are measured by ring electrodes inside a housing that allows borehole fluid to flow through. Best fluid resistivity logging results are achieved when logging downward into boreholes containing ambient water that has had sufficient time to stabilize. Ideally, fluid resistivity logs are run with temperature logs in static boreholes as the initial logging run to record the ambient conditions before other probes have passed through the borehole and vertically mixed the borehole fluid. Curve deflections on the fluid resistivity and temperature logs can be an indication of horizontal or vertical flow movement, of stratification of borehole fluid, or of screen openings in cased wells. The fluid resistivity values can also be used in calculations with other logs.

A Mount Sopris Instrument model number 2PFA-1000 temperature-fluid resistivity probe was used to log fluid resistivity and temperature in the monitoring wells as the initial logging run. The fluid resistivity logging probe was calibrated with solutions of known conductivity in a two-point calibration. Temperature is calibrated at the factory and required no field calibration during this investigation.

Electromagnetic Induction Logs

The EM induction probes measure conductivity in air-filled or water-filled holes and perform well in open or PVC-cased holes; metallic, conductive objects interfere with the electromagnetic field. The measurement of conductivity is commonly reciprocated to provide logs with curves of both resistivity and conductivity (Keys, 1997), as was done with the logs in this study. Conductivity can be affected by the salinity of borehole and formation fluids and by the type of lithology encountered. Generally, pure carbonates, sands, and gravels have a lower conductivity (thus a higher resistivity) than clays or shales (Keys, 1997).

A Geonics EM39 induction conductivity probe (Geonics Limited, Mississauga, Canada) was used on all wells. The EM39 was calibrated twice daily using manufacturer's recommended procedures (Mount Sopris Instrument Co., 2002) at temperatures within the range expected in the boreholes. To attain a stable temperature, the probe was suspended in a well for 20 to 30 minutes prior to calibration. During the two-point calibration process, the probe was (1) calibrated to a zero conductivity environment, and (2) calibrated to a calibration coil of known conductivity with the bottom of the probe at least 3 m above the ground. The calibration was also checked periodically between the calibration procedures. The EM induction conductivity measurements were adversely affected at depths corresponding with metal objects such as centralizers and stainless steel screens. All EM induction logs collected during the investigation were run in accordance with the American Society for Testing and Materials standard guide (American Society for Testing and Materials, 2001).

Natural Gamma Logs

Natural gamma logs provide a record of gamma radiation detected at depth in a borehole. Fine-grained sediments that contain abundant clay tend to be more radioactive than quartz-grain sandstones or carbonates (Keys, 1997). The natural gamma and EM induction logs collectively can be very useful in determining lithologies and contact depths of the strata penetrated in the borehole. Natural gamma count rates, which will commonly increase in the proximity of clay and shale, could also be slightly increased adjacent to bentonite seals in the wells.

The natural gamma log was run subsequent to the fluid resistivity log, and data were recorded in natural gamma counts per second (cps). A Mount Sopris Instruments 2PGA-1000 natural gamma probe with a sodium iodide detector was used. The natural gamma probe is calibrated at the factory and does not require calibration in the field. All natural gamma logs collected during the investigation were run in accordance with the American Society for Testing and Materials standard guide (American Society for Testing and Materials, 2004).

Acoustic Velocity Logs

Acoustic velocity logs record the travel time of pulsed acoustic waves from a transmitter to one or more receivers. The acoustic pulse travels through the fluid in the well and through the surrounding rock at a velocity that is related to the lithology and porosity of the rocks (Keys, 1997). Consequently, the well must be filled with mud or water to transmit the acoustic energy to the borehole wall. The acoustic velocity probe must be centralized with bowspring or rubber centralizers to keep the travel path of the acoustic energy at a consistent length. A Mount Sopris Instruments model 2SAA-1000 sonic probe with a single transmitter and dual receiver system was used for recording the travel times of the formation. The receivers are spaced at 0.6 and 0.9 m from the transmitter. Therefore, a 0.3 m calculation was made to measure this interval transit time in microseconds per meter (μs/m), which is referred to as slowness.

The acoustic wave train received by the two receivers can be divided into several components, of which the most important are the compressional (P-) waves and shear waves. P-waves have a lower amplitude and higher velocity than shear waves (Keys, 1997). Generally, acoustic velocity logs record the travel time of the P-waves, or the first arrival of amplitude; we processed only for the P-wave velocities. The P-wave velocities were calculated using the WellCad 4.0 Full Wave Sonic processing module (Advanced Logic Technologies, 2004). This processing module scans the sampled data for the first arrival above a preset amplitude threshold for each receiver and calculates the slowness. The travel times for the individual receivers are used to compute the velocity analysis semblance plot, which is used to interpret coherent events between all receivers of the multi-receiver sonic tool. This process generates a slowness log that can be reciprocated to velocity to compare with the surface seismic methods. Acoustic logging data are subject to many sources of error such as large or irregular borehole diameter, poor centralization, cycle skipping, and unsaturated or highly unconsolidated formation material.

Surface Geophysical Methods

Direct-Current Resistivity

The direct-current (DC) resistivity method is used to determine the electrical resistivity structure of the subsurface. Resistivity is the property of a material that opposes the flow of electric current. The dominant factors in determining the resistivity of a soil or rock are typically the amount of interconnected water, water quality (based on total dissolved solids (TDS) levels), and the presence of mineralogical clay (for example, montmorillonite). An unsaturated rock will typically have a higher resistivity than a saturated rock, and the presence of water with high TDS or of high clay concentrations will decrease the bulk resistivity of a material. Thorough discussions of the resistivity technique and electrical responses of earth materials can be found in Butler (2005), Reynolds (1997), and Sharma (1997).

Direct-current resistivity measurements are made by inserting electrodes into the ground. Typically, each electrode is a solid stainless steel rod roughly 1.5 cm in diameter and 0.5 m long or less that is hammered into the ground and connected to the main control unit through a set of wires or cables. Four electrodes, two current-transmitting (current) and two voltage-sensing (potential), are required for each measurement. Our surveys combined two techniques: horizontal profiling and vertical sounding. Horizontal profiling is a method to determine lateral variations in earth resistivity within a limited depth range, and the electrode spacing and geometry are held constant as the array of four electrodes are moved along a survey line. Vertical sounding is a method to investigate the change in earth resistivity with depth at a particular location, and the electrodes are arranged symmetrically about a center point, with increasing distances between current and potential electrodes used to explore greater depths.

For each measurement, the resistance, R, is calculated using Ohm's Law (for example, Reynolds, 1997):

$$R = \frac{\Delta V}{I} \tag{1}$$

where

ΔV represents the potential difference measured by the potential electrodes,

and

I represents the current applied through the current electrodes.

The apparent resistivity of the subsurface is calculated by multiplying each resistance by a geometric factor determined by the geometry and the spacing of the electrode array. When the measured section is homogeneous and isotropic, the calculated apparent resistivity is the true resistivity of the section. When the measured section is heterogeneous and anisotropic, as is most often the case, the calculated apparent resistivity must be inverted to determine a best-fit layered-earth resistivity model of the subsurface (Loke, 2000).

Data Acquisition

The DC resistivity data were collected using a multi-electrode IRIS Syscal R1 Plus resistivity meter (IRIS Instruments, Orleans, France). Six resistivity lines were acquired: three lines in the upland portion of the study area and three in the floodplain (fig. 2). The lines were located based on proximity to the source area, general hydraulic gradient between the source area and the Meramec River, and accessibility. The basic setup for the lines included laying out 72 stainless steel electrodes with various electrode spacings (table 1). For lines extending beyond the initial layout of 72 electrodes, we "rolled-along," or moved, sets of 12 electrodes, one set at a time, from the front of the line to the end, thereby extending the line length without sacrificing resolution at depth. All lines were collected using a Wenner-Schlumberger array. During acquisition of Line 2, an electrode position at 480 m was skipped, such that the overall line length was 570 m but should have been 567.5 m. These data were post-processed to correct this acquisition geometry error before inversion. We also experienced a brief equipment malfunction on Line 2 that created a gap in our data coverage. This gap is shown in the raw data pseudosection in appendix 2, and as a result, our interpretations of fine details observed in the data in this area are limited.

Data Inversion

An inversion program uses the DC resistivity data from a given line to develop a 2D model consisting of rectangular cells of individual resistivity values. The program determines the calculated system response of the model, which is referred to as the calculated apparent resistivity, on the basis of the field collection parameters such as the array type and electrode spacing. The root-mean-square (RMS) difference between the measured and calculated apparent resistivity profiles is used to determine the accuracy of the model. The inversion program then attempts to reduce the RMS difference by altering the model resistivity values and recalculating the apparent resistivity, effectively attempting to match the collected field data. When the RMS difference between the calculated and measured apparent resistivity no longer improves between iterations by a user-specified percentage of the total RMS difference, a solution is reached. The final model represents a non-unique estimate of the probable distribution of electrical resistivity within the subsurface. This inversion process is described in detail by Loke (2004).

The DC resistivity data were inverted using the program RES2DINV version 3.55.49 from Geotomo Software (Loke, 2004) using the finite-element method with the least-squares approximation. Data were topographically corrected using a combination of global positioning system (GPS) and leveling elevations. The apparent resistivity pseudosections (a plotting convention for apparent resistivity data that should not be

Table 1. Summary of direct-current resistivity acquisition parameters. Lines 1, 3, and 4 are located in the upland site, and Lines 2, 5, and 6 are located in the floodplain site.

Line	1	2	3	4	5	6
Total no. electrodes	72	228	72	96	156	144
Electrode spacing	2 m	2.5 m	1.5 m	1.5 m	1.5 m	1.5 m
Total line length	142 m	570 m	106.5 m	142.5 m	232.5 m	214.5 m
Measurement time	250 ms					
Array type	Wenner-Schlumberger					

considered a cross section) and inversion results are given in appendix 2 for all six lines. Once the DC resistivity data were inverted, the profiles were input into the software package Profile Analyst (Encom, 2004) to view the three-dimensional (3D) spatial relationships between adjacent profiles.

Seismic Refraction

The seismic method uses elastic, or sound, waves to delineate subsurface variations in compressional and shear velocity. These velocities are dependent on properties such as bulk modulus, shear modulus, and density that vary with rock or soil type. There are two main types of seismic waves: body waves and surface waves. Body waves travel through the bulk of the subsurface media and include P-waves (seismic energy in which the particle motion is parallel to the direction of energy propagation) and shear waves (seismic energy in which the particle motion is perpendicular to the direction of energy propagation). Surface waves propagate only along material interfaces (Reynolds, 1997).

Surface seismic profile data are acquired with a seismic source (for example, sledgehammer or explosive charge) and multiple receivers, or geophones, laid out in a linear array, that record particle motion as a function of time. Seismic data include body and surface wave energy created by the source as well as background noise or energy from other unwanted sources (for example, overhead planes, cars, and wind). By recording data with multiple source and receiver locations, the measured section can be more accurately imaged seismically through data redundancy. For more detailed information on the seismic method, refer to Telford and others (1990), Reynolds (1997), and Butler (2005).

Refraction analysis of seismic data tends to give a more general picture of the subsurface layering as velocity variations with depth and distance, whereas reflection surveys have the ability to image much greater stratigraphic detail. Reflection data, however, require media that support reflected wave energy and require much more processing to get a final image. When simpler details such as the bedrock surface are the target of the survey, refraction analysis can be sufficient.

Data Acquisition

The P-wave seismic refraction data were acquired using two Seistronix RAS-24 seismographs (Seistronix, Rancho Cordova, Calif.) with a 4.5-kg sledgehammer and brass plate source. To prevent poor-quality shots from being included in a field-stacked record, at least two unstacked shot records were recorded at each station and stacked later during data processing. Each shot was analyzed to determine the need for additional shots as data were collected. In general, the data collected at the upland site have a greater signal to noise ratio than the floodplain data. In particular, all of Lines 5 and 6 and the eastern half of Line 2 were acquired along monitoring well access roads located in the woods. The main source of noise in the floodplain data was caused by the tall trees swaying in the wind that created noise in the ground by the vibrations of the tree roots. To help minimize noise from trains passing on the two nearby active railroad tracks and frequent low-flying planes, acquisition was suspended momentarily until these noise sources had passed.

The six seismic refraction lines are located coincidentally with the positions of the DC resistivity lines (fig. 2). Each line segment, consisting of a single, fixed 48-geophone spread, was acquired with shot points located midway between each geophone and with off-end shots that have a shot spacing range of 1 to 5 stations (1 to 10 m). The survey used station numbers, a typical record-keeping convention for seismic data acquisition. For each of the seismic lines, the station spacing is equivalent to the geophone spacing, and station 1 is always located at the first (westernmost) geophone location. When the total length of the line required more than one 48-geophone line segment, multiple 48-geophone spreads were acquired incrementally either end-to-end or with a 12-geophone overlap. Shot stations were continued past the last geophone by one-quarter of the spread length, which increases the subsurface coverage between the line segments in a more efficient manner than increasing the geophone overlap. All three upland lines were acquired with a geophone spacing of 1 m. In the floodplain, we increased our geophone spacing to get greater depths of penetration. Table 2 summarizes the acquisition parameters for all six seismic lines.

Table 2. Summary of seismic refraction acquisition parameters. Lines 1, 3, and 4 are located in the upland site, and Lines 2, 5, and 6 are located in the floodplain.

Line	1	2	3	4	5	6
No. geophones	48	240	86	144	144	96
Geophone/station spacing	1 m	2.5 m	1 m	1 m	1.5 m	1.5 m
No. shots	53	333	107	176	176	110
Shot spacing	1 m	2.5 m	1 m	1 m	1.5 m	1.5 m
Line geometry	1 48-geophone spread	5 end-to-end 48-geophone spreads	2 48-geophone spreads w/ 12 overlap	3 end-to-end 48-geophone spreads	3 end-to-end 48-geophone spreads	2 end-to-end 48-geophone spreads
Total live line length	47 m	597.5 m	85 m	143 m	214.5 m	142.5 m
Record length	500 ms					
Sample rate	0.25 ms					
Geophone type	40 Hz P-wave					
Source type	4.5-kg sledgehammer & brass plate					

Historically, standard seismic refraction survey procedures included the acquisition of only a few shot locations, typically one shot at either end of the geophone spread and one to three more spaced equally within the spread. The resultant velocity model was a basic representation of the subsurface structure with generally low lateral resolution. With the advent of various refraction tomography software packages, a more densely acquired shot geometry can lead to much higher lateral velocity resolution and possibly even the imaging of discontinuous velocity inversions (when a slower velocity layer underlies a faster velocity layer). This method has been successful at several field sites, based on correlation with available borehole data, through the use of the dense acquisition geometry and commercially available refraction tomography software (for example, Powers and others, 2007; Powers and Burton, 2007).

Data Processing and Inversion

The seismic refraction method requires little data processing. The raw shot records acquired in the field can be used to determine the arrival times of the first recorded energy, or first break, at each geophone. The P-wave refracted wave is typically the first energy generated by the source received by the geophones. The first break picks are recorded for each geophone at every source location. Figure 3 shows a sample shot record from each of the six seismic lines with the first break picks displayed.

For each shot, the first break picks are plotted versus increasing source-receiver offset distance to create a single traveltime curve. Changes in the slope along these curves at later times indicate variations in apparent velocity of arriving energy. Through the utilization of modeling software using the first break picks, a best-fit velocity model of the subsurface can be determined. This velocity model can then be interpreted to determine a probable geologic model.

We manually picked the first breaks on the cleanest raw, unstacked shot record at each shot station. Only the traces with high pick confidences were picked; exceptionally noisy traces were skipped. The resultant traveltime curves are shown for each of the lines with the acquisition geometries in appendix 3. The degree of curve parallelism indicates the quality of the first break picks and can be an indicator of overall data quality.

The first break picks were modeled using the software package Rayfract by Intelligent Resources, Inc. (Intelligent Resources Inc., 2006). The initial velocity model was obtained using the smooth inversion Delta-t-V turning ray method (Gebrande and Miller, 1985) with the one-dimensional (1D) gradient option. The standard Delta-t-V method produces a pseudo-2D model with lateral velocity changes along the profile. The smooth 1D gradient option is an average of all traces of the pseudo-2D model and is the recommended starting model to minimize velocity artifacts in the final model (Intelligent Resources Inc., 2007). Subsequent model refinement was performed using the 2D wavepath eikonal traveltime (WET) tomographic inversion method (Schuster and Quintus-Bosz, 1993). These final inversion profiles were also input to Profile Analyst to view in 3D space with the DC resistivity profiles.

Surveying Methods

The resistivity and seismic lines and monitoring wells were surveyed with a Trimble 5700 (Trimble Navigation Ltd., Sunnyvale, Calif.) real-time kinematic GPS to determine their location and elevation, supplemented with a Sokkia SDL30 digital level system (Sokkia Co., Ltd., Atsugi, Japan) in forested areas unsurveyable with GPS. Horizontal coordinates are presented in the North American Datum of 1983 (NAD83) Universal Transverse Mercator (UTM) Zone 15 North projection. Elevations are referenced to the North American Vertical Datum of 1988 (NAVD 88).

Identifying Preferential Flow Paths

A monitoring well program was first established in 1998 to determine dominant contaminant flow paths in AOC 2. The results of their measured contaminant concentrations of TCE and DCE (table 3), however, did not lead to a conclusive model of what was happening in the subsurface between the source area and the wells to indicate high contaminant concentrations. Monitoring well 33, which is located closest to and downgradient from the source area (fig. 2), had a measured TCE concentration ten times less than that of MW21, located further downgradient. Located in the floodplain, MW26 had the next highest contaminant levels, while MW34 had relatively low concentrations. In this investigation, the monitoring well information and the geophysical data were used to better understand the contaminant transport processes.

The DC resistivity and seismic refraction results are presented as geophysical profiles with available lithology and borehole logs of nearby monitoring wells. For plotting purposes, we applied an 11-point running average filter to each of the logs to better demonstrate general trends in the geophysical profiles. Figures 4 through 10 contain the lithology and unfiltered borehole logs in greater detail for each of the accessible monitoring wells, including MW23, which is not shown with any of the geophysical profiles.

Direct-Current Resistivity Results

The geophysical profiles will be described in order from south to north, which also corresponds with the topographically highest to the lowest toward the floodplain of the Meramec River (fig. 2). All six DC resistivity profiles exhibit an increasing resistivity trend with depth and have undulatory variations in the interpreted bedrock topography. There is a gradational increase in resistivity; therefore, a distinct top of bedrock contact is difficult to identify.

In the upland site, there are three geophysical profiles presented: Line 3, Line 1, and Line 4, from south to north (fig. 11). At the upland site, there is generally a 10-m-thick upper layer with a consistently low resistivity of 100 ohm-m or less. Line 3 shows an upper layer, characterized by discontinuous

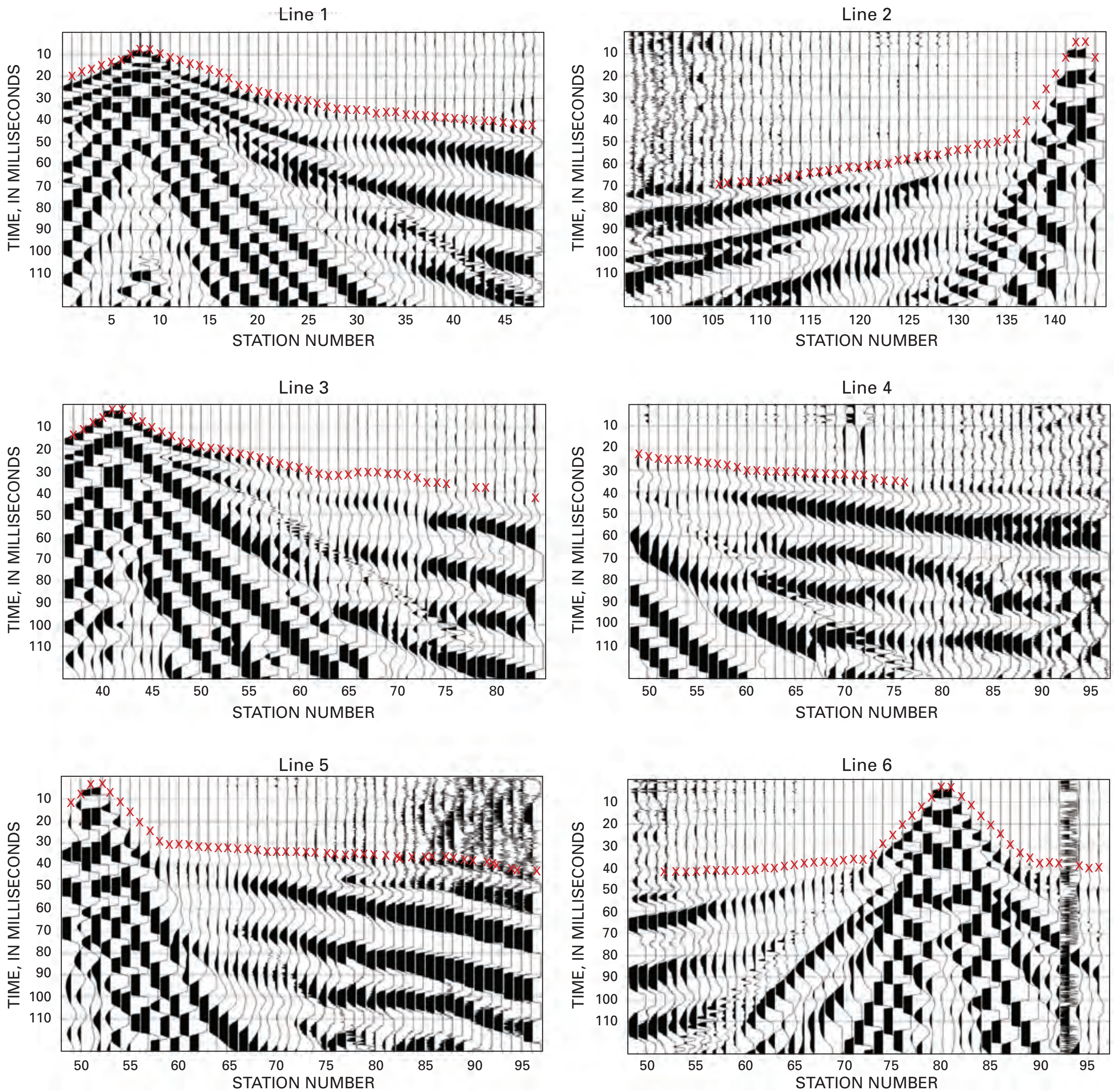

Figure 3. Sample raw shot records from each of the six seismic refraction profiles; the only process applied normalizes the amplitudes for each trace to aid in picking first breaks. The red x on each trace indicates the first break pick.

low- to moderate-resistivity, that extends from the surface to a depth of about 2–3 m; it is interpreted to be a chert or chert-rich clay layer. During acquisition, this line had the most notable indication of chert, or some other hard material, at the surface along the western half. The top layer is underlain by very low-resistivity sediments (30 ohm-m or less) that are about 5 m thick. Below about 7–8 m depth, resistivity steadily increases with depth, which corresponds with weathered to competent limestone bedrock. The high-resistivity anomaly near the surface at 94 m is most likely an artifact from some unknown buried object. The cause of the two resistive spires at 30 and 60 m that protrude from the bedrock toward the surface is unknown, but it should be noted that their positions roughly correlate with the ends of a 1- to 2-m-high forested berm that is located between the source area and Line 3 (fig. 2).

Line 1 exhibits a discontinuous layer at the surface that extends to about 3–4 m in depth and is interpreted to be the same chert or chert-rich clay layer observed along Line 3. This layer is underlain by a very low-resistivity layer (30 ohm-m or less) that is about 8 m thick (fig. 11). Below about 11–12 m depth, resistivity steadily increases with depth.

Line 4, the northernmost profile in the upland site, shows evidence of the same near-surface layer seen in the other two profiles with a resistivity around 80–100 ohm-m. This layer,

Table 3. Summary of measured monitoring well contaminant concentrations and specific conductances (MicroPact, 2006). The blue monitoring wells are located in the upland area, and the yellow monitoring wells are located in the floodplain (see fig. 2). ND (non-detect) indicates that the concentrations were below the detection limits of the measuring instrument.

[TCE, trichloroethylene; DCE, dichloroethylene]

Monitoring well	TCE[1] (μg/L)	DCE[2] (μg/L)	Specific conductance (μS/cm)
MW19	6.4	0.42	232,000
MW20	210	510	Dry
MW21	26,000		422
MW23	ND	ND	773
MW24	ND	ND	146,000
MW25	5.2	4	420,000
MW26	350	220	420,000
MW27	ND	ND	936,000
MW28	0.23		205,000
MW29	3.1	1.1	523
MW30	4.8	8	283
MW31	ND	ND	392
MW32	38	66	247
MW33	2,500	540	533,000
MW34	52	0.8	568
MW35	ND	ND	430

[1]TCE maximum contaminant level = 5 μg/L (U.S. Environmental Protection Agency, 2006a).

[2]DCE maximum contaminant level = 7 μg/L (U.S. Environmental Protection Agency, 2006b).

however, is less distinct than in the other two profiles, except on the eastern side, where it appears to be deeper (down to about 5 m depth) than in the other profiles (fig. 11). The thickness of the low-resistivity upper layer varies from about 6 to 8 m, and the high-resistivity lower layer dips toward the east with a shallow depression centered at 95 m.

In the floodplain site, there are three more geophysical lines of data presented: Line 5, Line 6, and Line 2, from south to north (fig. 12). The floodplain site resistivity results have a different character because of the presence of coarser alluvial deposits (sand and gravel) that were not present at the upland site, where the soil consists mostly of silt and clay with chert. Lines 5 and 6 have a similar appearance with a 4- to 8-m-thick low-resistivity layer of 100 ohm-m or less overlying an undulatory higher-resistivity layer, which is likely bedrock. This lower layer exhibits multiple zones of decreased resistivity values that correspond with the undulations observed along the 650-ohm-m contour.

Line 2 is the closest line to the current Meramec River channel and is about 300 m north of Lines 5 and 6. This line exhibits a thin, low-resistivity layer at the surface, about 2–4 m thick, underlain by a very high resistivity layer (greater than 1,300 ohm-m) 8 to 12 m thick (fig. 12). Below this resistive layer is a slightly more conductive and more heterogeneous layer that is somewhat similar in character to the resistive layer at depth in Lines 5 and 6. The source of the two near-surface anomalies centered at 15 and 390 m is interpreted to be related to either natural drainage or manmade features such as a buried pipeline or trench, which are visible on the aerial photographs of the site. Figure 13 is similar to figure 2 but uses an older, lower resolution aerial photograph that better shows a linear trend in the trees that corresponds with the anomaly at 390 m. The resistive nature of the anomaly at the surface indicates either a less clay-rich deposit that becomes more conductive with depth below the water table or simply a strong anomaly artifact from some type of near-surface buried item.

Seismic Refraction Results

All six profiles generally exhibit increasing velocities with depth. The downline distances plotted on the seismic profiles (figs. 14 and 15) are relative to the positions of the respective DC resistivity profiles (for example, 70 m on DC resistivity Line 1 corresponds to the 70 m distance on seismic Line 1). The color scale is chosen to help show typical velocities for unsaturated, unconsolidated regolith (white to tan: 0 to 1,500 m/s); saturated, unconsolidated or unsaturated, partially consolidated regolith (blue to purple: 1,500 to 3,000 m/s); and consolidated rock (red to black: 3,000 to 6,000 m/s). Based on the velocity images, the thickness of the unconsolidated to partially consolidated regolith in the upland site varies from about 15 to 20 m (fig. 14). Below that is a layer that is increasingly consolidated with depth. The maximum depth of investigation is determined by the maximum depth of penetration of the raypaths. The inconsistent maximum depth of investigations displayed in figures 14 and 15 are due to a combination of artifacts of the acquisition geometry and of changes in the maximum depth of penetration of the modeled raypaths.

Delineating between partially consolidated regolith and fractured or weathered bedrock can be difficult because their seismic velocities are similar. When interpreting these refraction profiles, we interpret the top of bedrock, in this case limestone, to be at around 3,500 m/s. A rock with this velocity must physically be very competent and of high quality. What lies above this contour may be limestone but, based on the seismic velocities, is not competent and is probably weathered/highly fractured. With the aid of the geophysical and driller's logs, the regolith/weathered limestone contact, as well as the seismically-defined competent limestone, can be better defined.

Based on the 3,500 m/s definition of competent bedrock, depth to competent limestone along Line 3 ranges from about 14 to 23 m (fig. 14). The limestone rises in the center of the profile about 4–5 m above the contact on either side. The bright red contours between about 3,000 and 3,500 m/s indicate varying degrees of weathered or fractured rock that changes laterally. Line 1 shows a relatively flat, competent limestone contact at around 18–20 m below the surface. The longest of the three upland lines, Line 4, shows a variably and gently sloping competent limestone with depths ranging from 15 to 20 m.

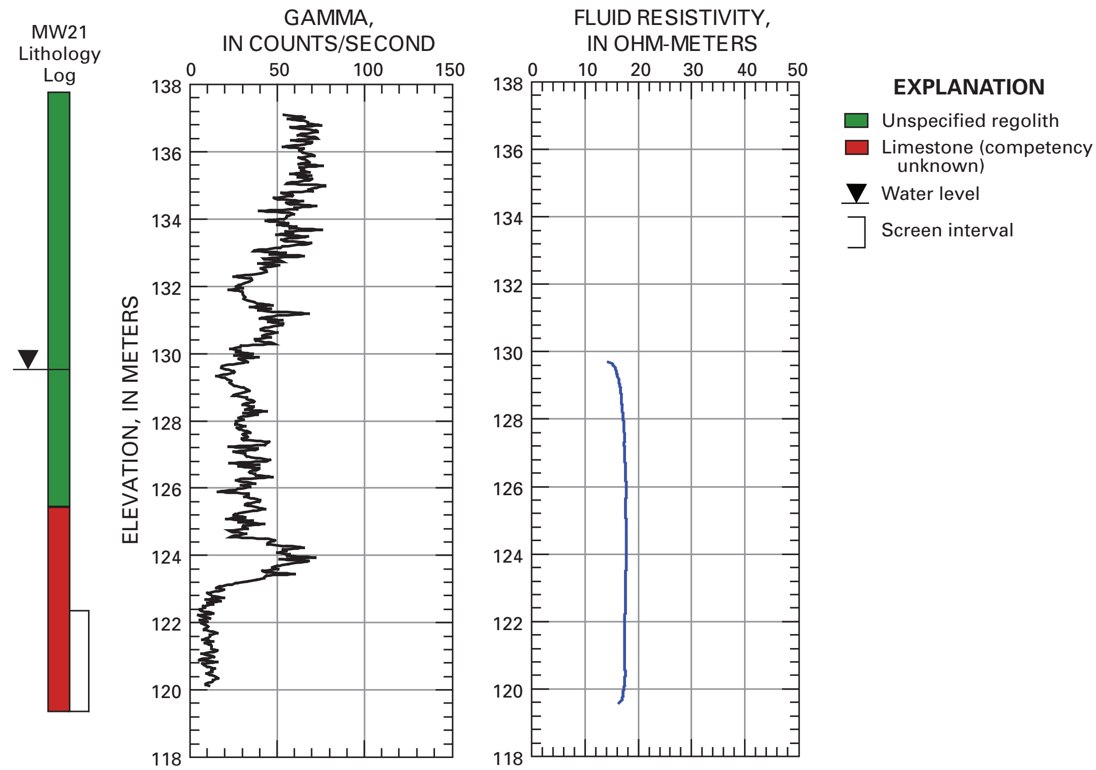

Figure 4. Lithology and borehole logs of MW21.

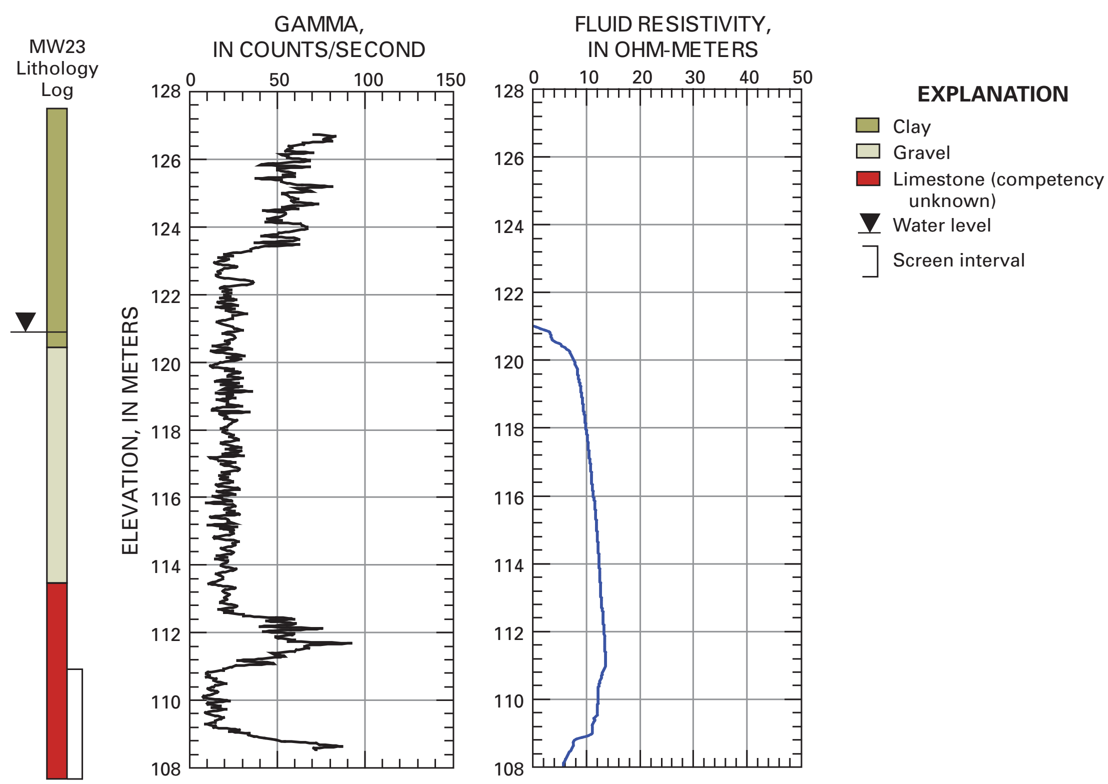

Figure 5. Lithology and borehole logs of MW23.

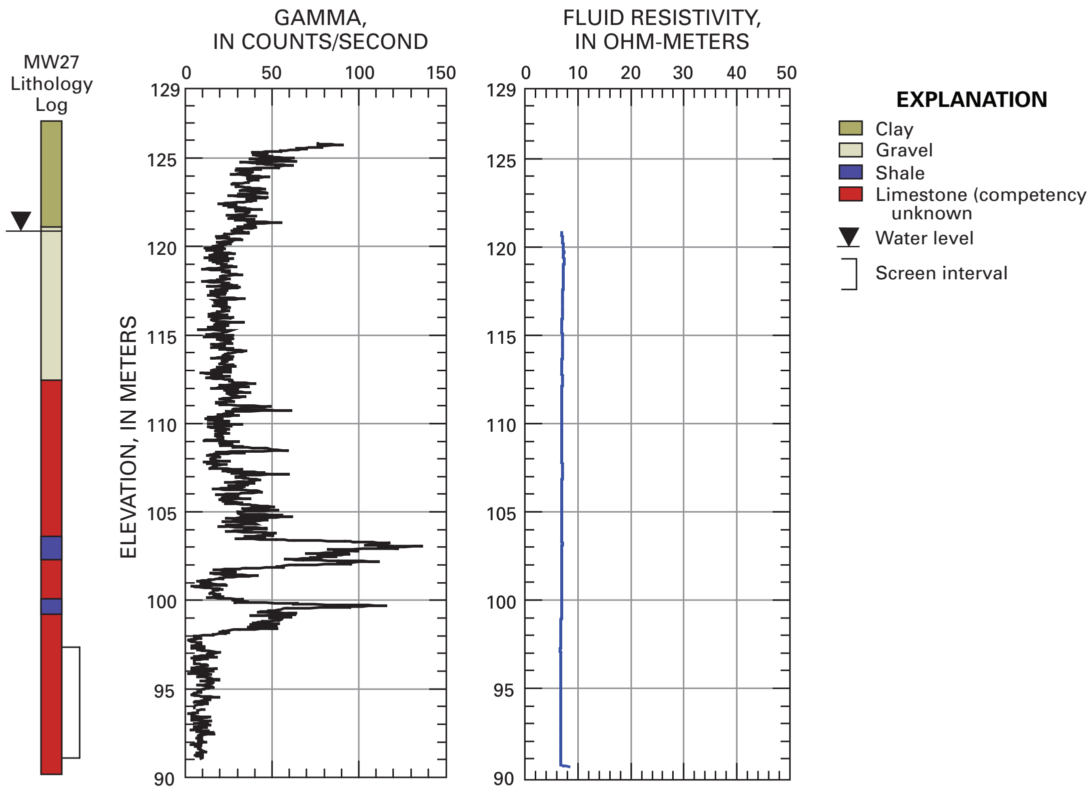

Figure 6. Lithology and borehole logs of MW27.

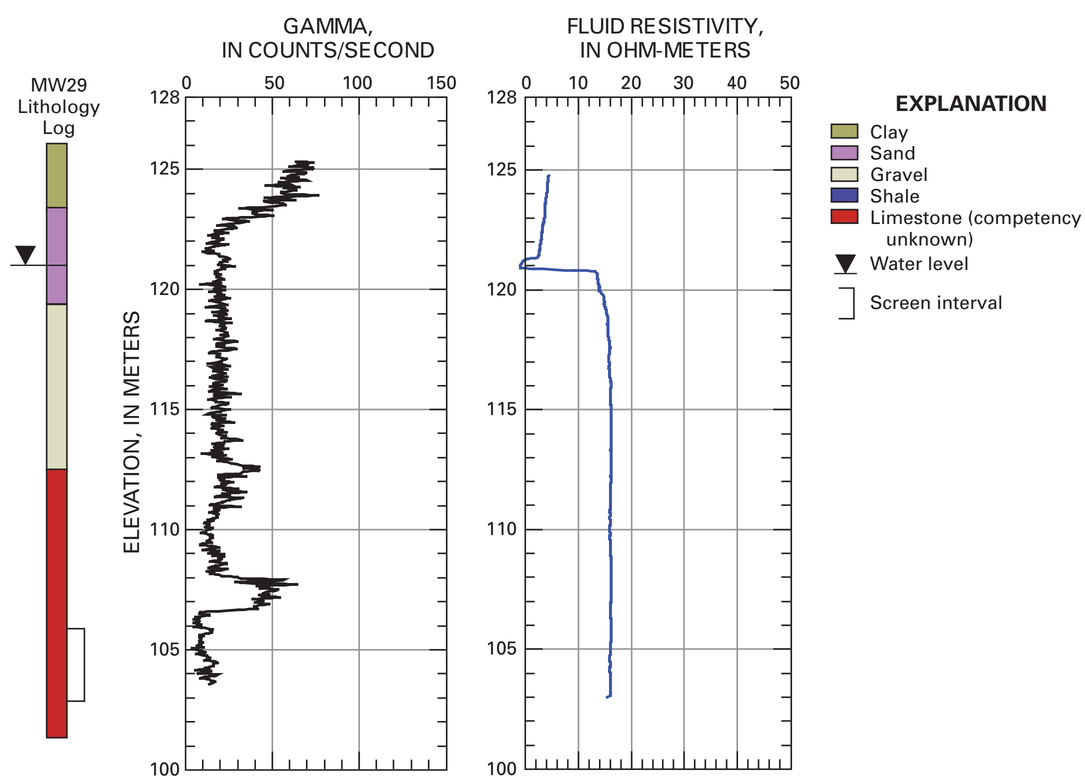

Figure 7. Lithology and borehole logs of MW29.

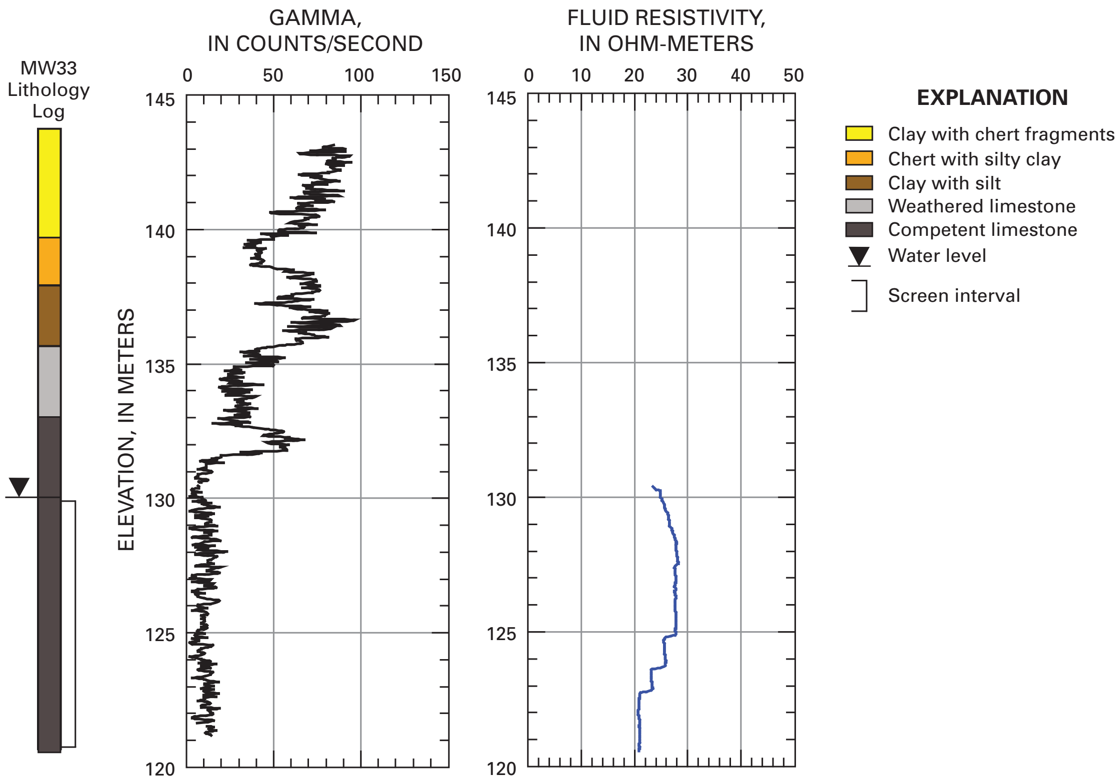

Figure 8. Lithology and borehole logs of MW33.

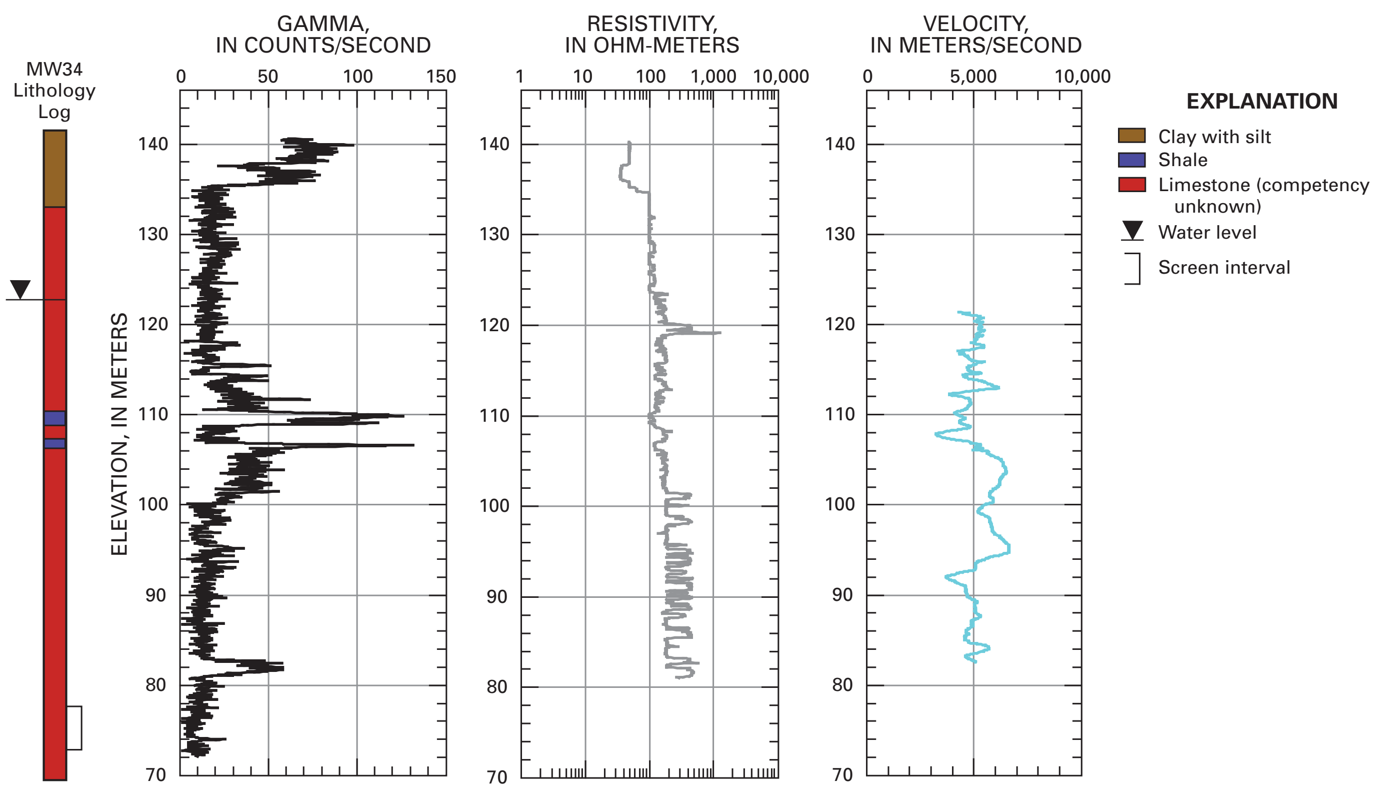

Figure 9. Lithology and borehole logs of MW34.

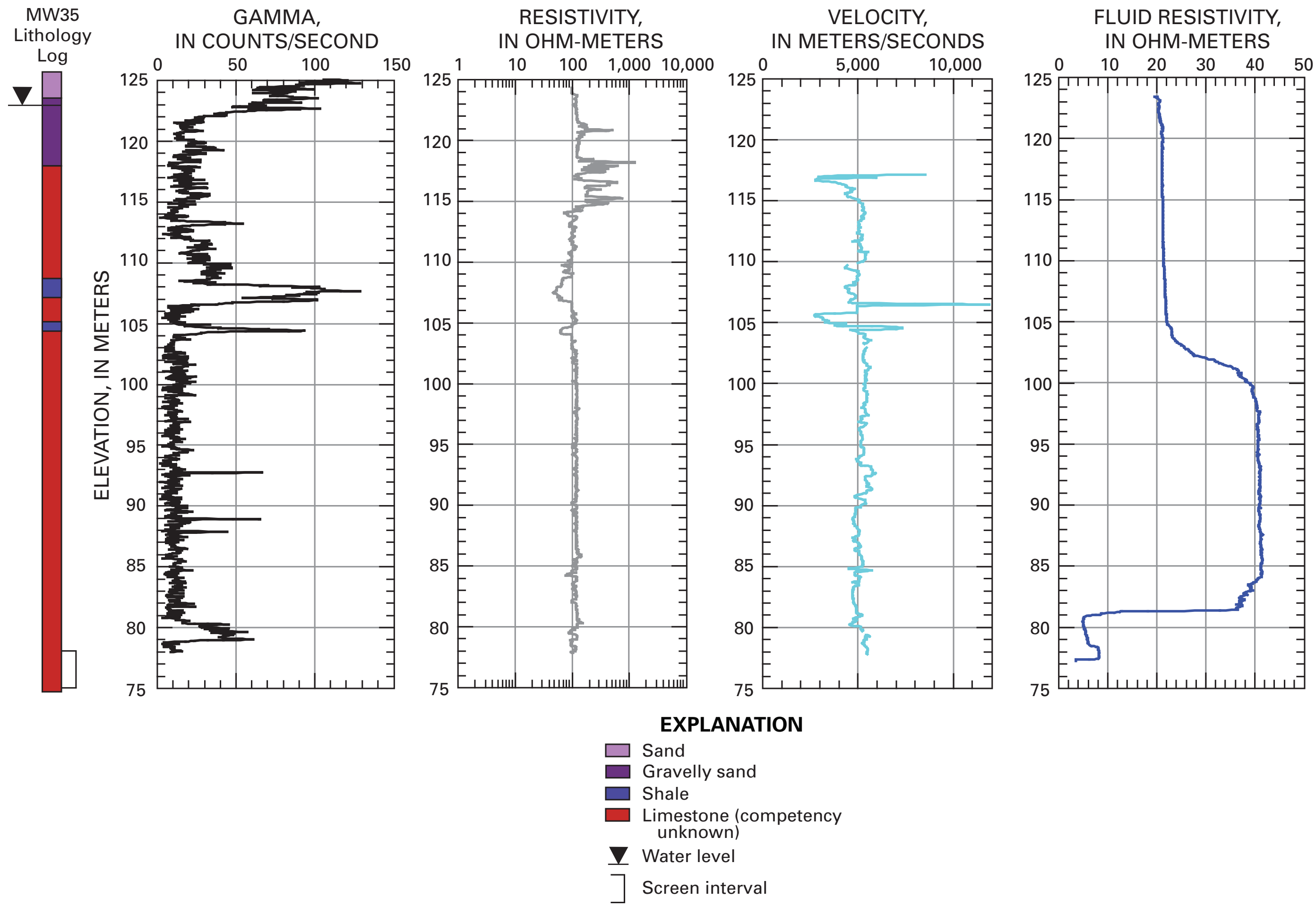

Figure 10. Lithology and borehole logs of MW35.

As with the DC resistivity results, seismic Lines 5 and 6 show similar character to one another, with an alluvium thickness of 10–15 m overlying the limestone bedrock (fig. 15). The good correlation of velocity structure over the zone of overlap between these two lines makes us confident in our results because we processed and inverted these two lines independently. The alluvium/limestone contact has an undulatory appearance for Lines 5 and 6 but appears generally flatter in Line 2. The thickness of the alluvium along Line 2 increases to about 15 to 20 m.

Integrated Interpretation of Geophysical Results

The process of interpreting the geophysical borehole and surface data in order to provide geologically meaningful results is highly dependent on the information gained from the available monitoring-well drilling records. The degree of correlation between the borehole and lithology logs is important for identifying lithologies and boundaries that can be extrapolated along the geophysical profiles away from the monitoring wells. The lithology logs presented in this report are based on well construction reports, certification records, and soil borings, which contain varying degrees of detail and are from several generations of monitoring well emplacements (MicroPact, 2006). Water levels were measured during the geophysical logging in May 2006.

Interpretation of Competent Limestone

It is important to identify the surface of competent limestone in the geophysical data because of the probable effect of the bedrock surface on DNAPL flow. Resistivity values for limestone can vary greatly, from 10^1 to 10^7 ohm-m (Reynolds, 1997; Sharma, 1997), depending on the degree of weathering and fracturing and on pore fluid quality. This variability and the gradational appearance of the resistivity profiles make it difficult to pick the top of competent limestone based on the induction logs or resistivity profiles. Instead, we used the natural gamma logs, the soil boring logs, and seismic velocities to determine the majority of the top of competent limestone interpretation.

We defined the top of competent limestone using the P-wave seismic interval velocity of 3,500 m/s because a rock that can support such a high velocity must be competent (figs. 14 and 15). The 3,500 m/s contour roughly corresponds with the 650-ohm-m contour of the DC resistivity profiles (figs. 11 and 12). These

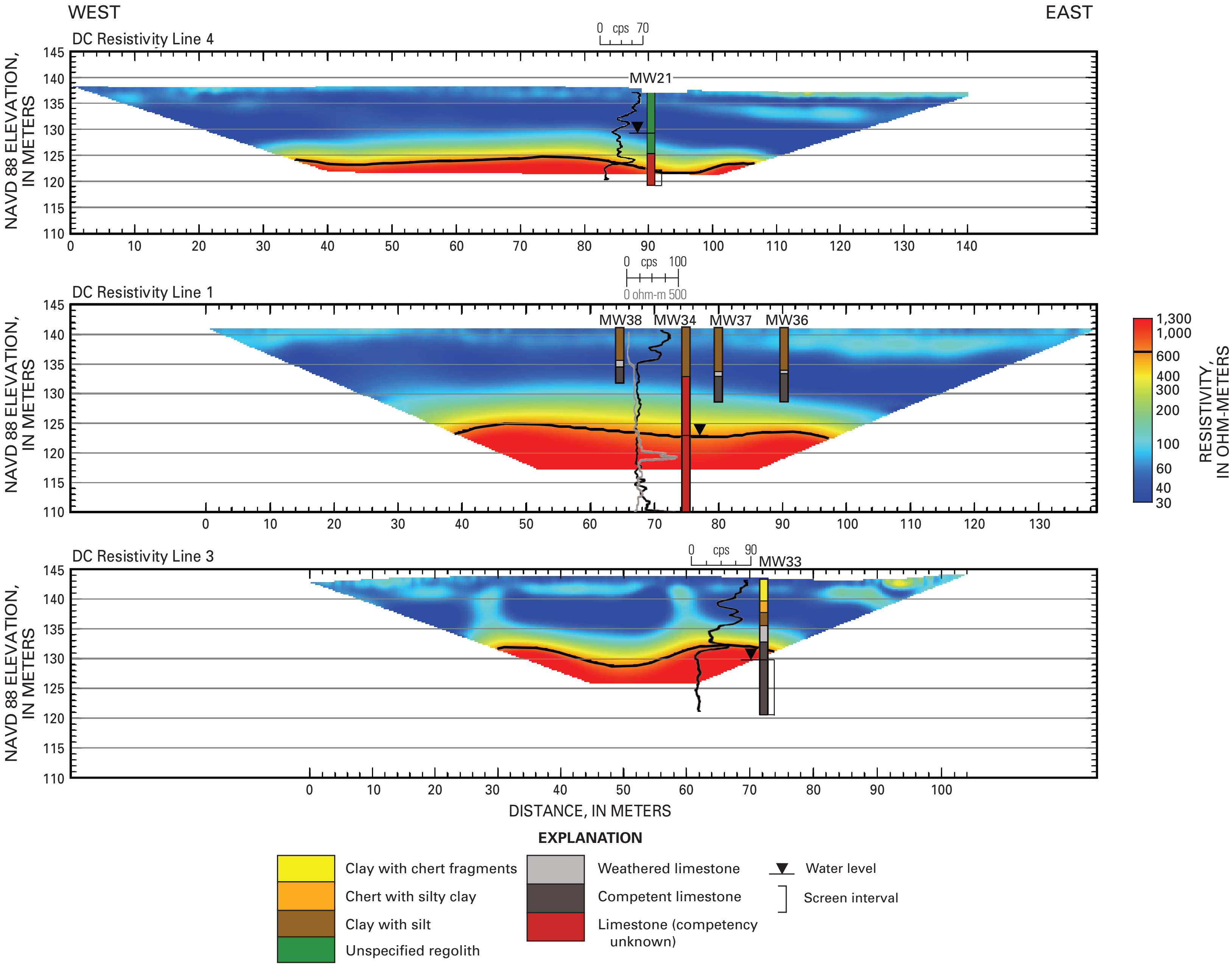

Figure 11. The three upland direct-currrent resistivity profiles shown with available geologic well information. The natural gamma logs (black; counts/second (cps)) are shown for MW21, MW33, and MW34, as well as the resistivity (gray; ohm-meters (ohm-m)) log for MW34. The horizontal solid black line on the profiles is the 650-ohm-m contour. (NAVD 88, North American Vertical Datum of 1988.)

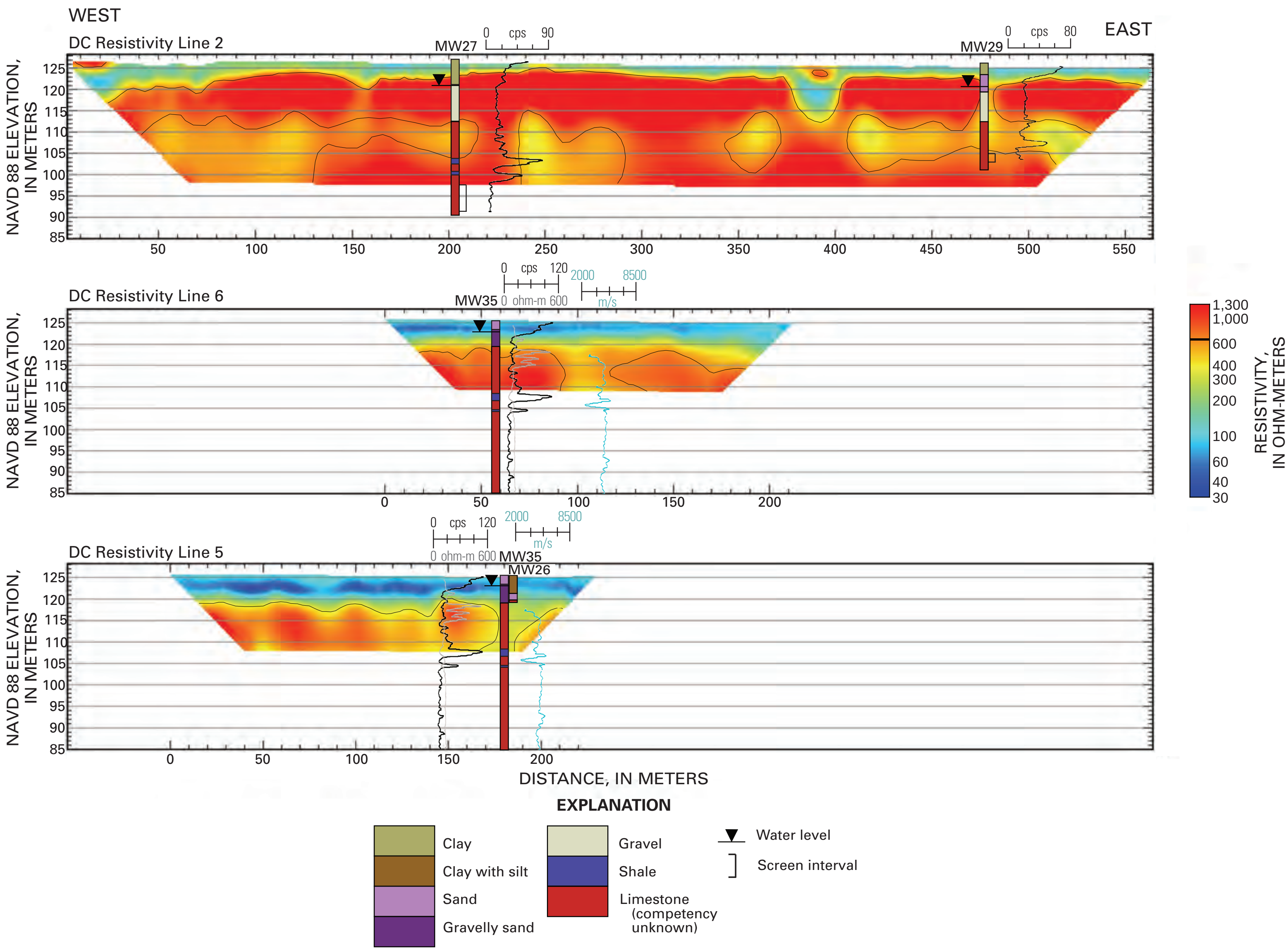

Figure 12. The three floodplain direct-current resistivity profiles shown with available geologic well information. The natural gamma logs (black; counts/second (cps)) are shown for MW27, MW29, and MW35, as well as the resistivity (gray; ohm-meter (ohm-m)) and sonic (turquoise; meters/second (m/s)) logs for MW35. The solid black line on the profiles is the 650-ohm-m contour. (NAVD 88, North American Vertical Datum of 1988.)

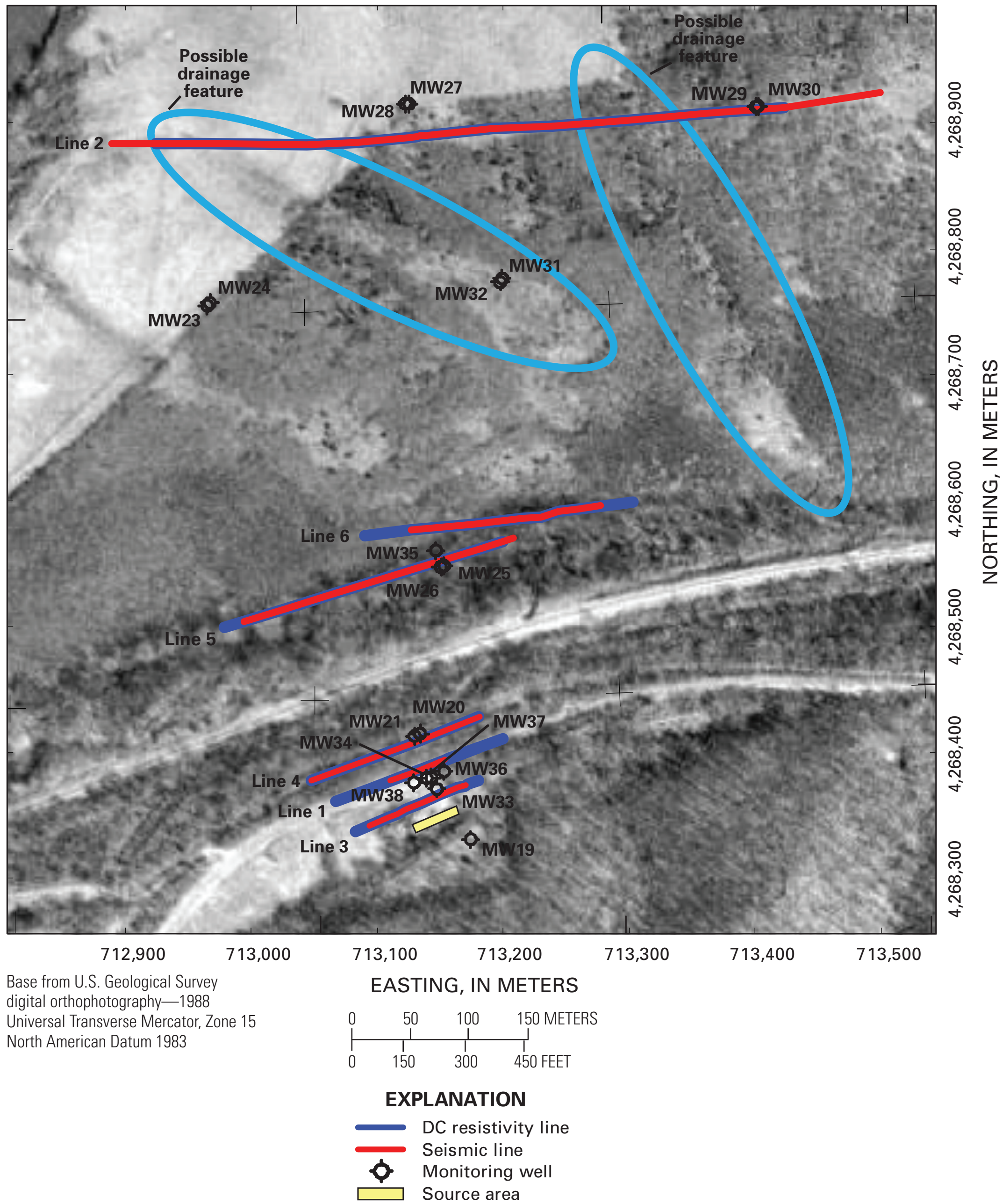

Figure 13. Aerial photograph of the upland and floodplain sites of AOC 2 of the former TVPF showing the locations of the six direct-current resistivity (blue) and seismic refraction (red) lines, nearby monitoring wells, approximate source area (yellow rectangle), and two features possibly related to two near-surface resistivity anomalies observed along Line 2 (blue ovals).

definitions result in an overall depth to competent limestone at the upland site of about 15–20 m with the shallowest limestone in the middle of Line 4. At the floodplain site, the depth to competent limestone ranges from 12 to 20 m.

Upland Site

With respect to geophysical interpretation, the upland site (near the contaminant source area) can be broadly defined as having the following lithologies:

1. regolith near the surface, about 8 to 12 m thick, clayey and silty for the most part with discontinuous lenses and layers of cherty fragments—within a few meters of the surface, the material is generally more resistive than lower materials;
2. weathered limestone bedrock, which is often identified as bedrock in the lithology logs, about 5 to 10 m thick; and
3. competent limestone bedrock, the surface of which is usually lower than the bedrock surface identified in the lithology logs.

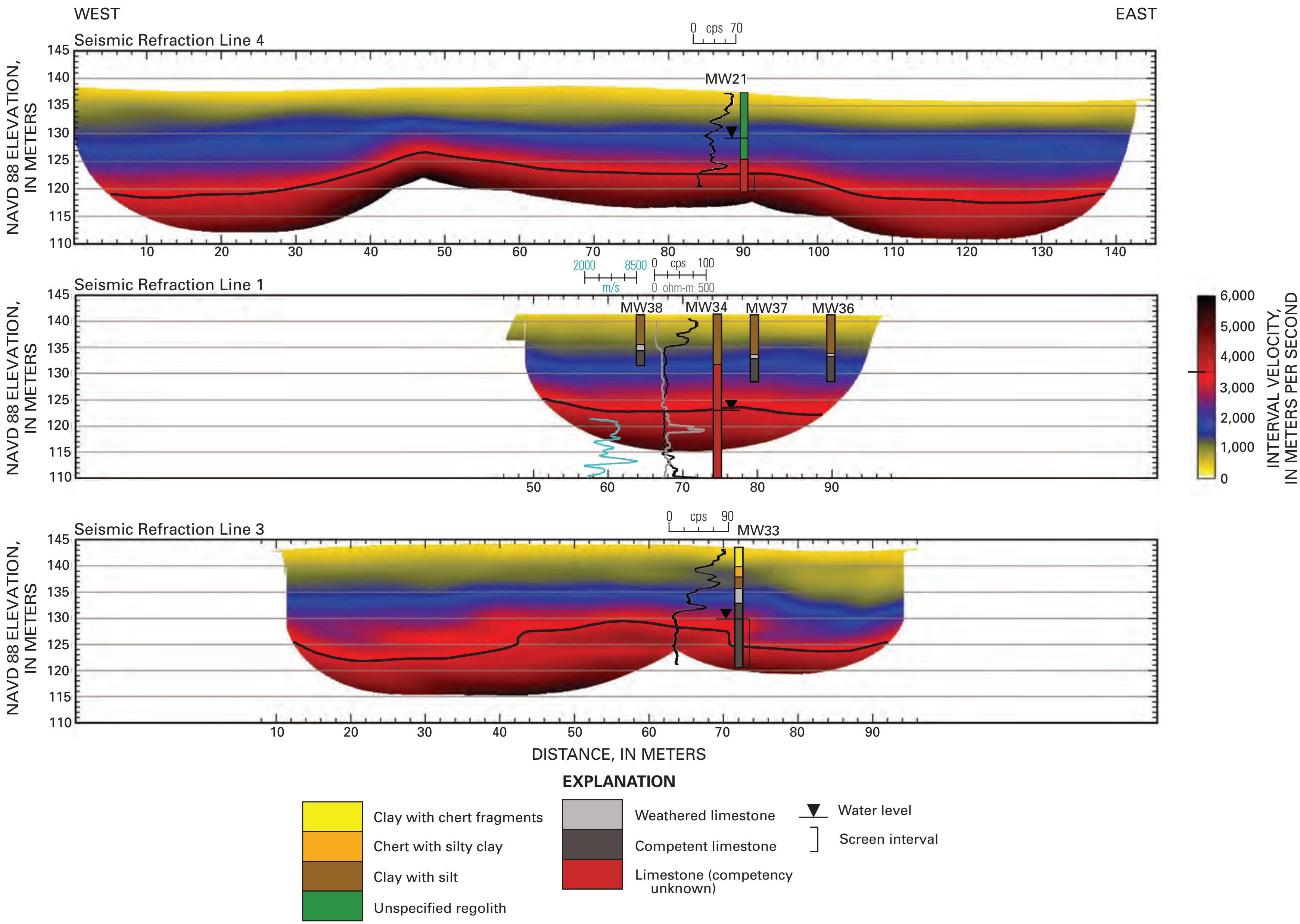

Figure 14. The three upland P-wave seismic refraction profiles shown with available geologic well information. The natural gamma logs (black; counts/second (cps)) are shown for MW21, MW33, and MW34, as well as the resistivity (gray; ohm-meters (ohm-m)) and sonic (turquoise; meters/second (m/s)) logs for MW34. The solid, black line on the profiles is the 3,500-m/s contour. The downline distances of the seismic profiles are relative to the positions of the respective direct-current resistivity profiles. (NAVD 88, North American Vertical Datum of 1988.)

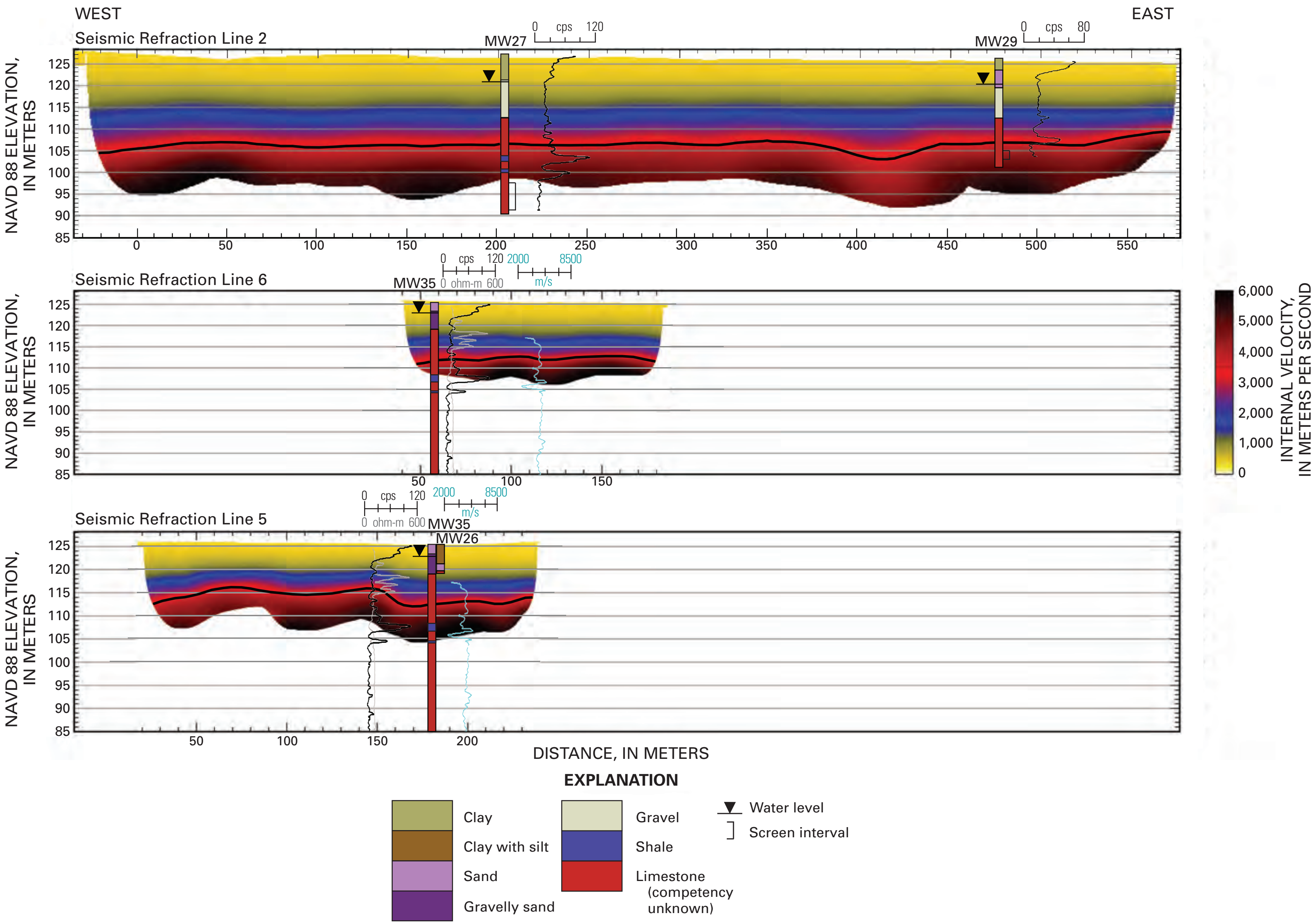

Figure 15. The three floodplain P-wave seismic refraction profiles shown with available geologic well information. The natural gamma logs (black; counts/second (cps)) are shown for MW27, MW29, and MW35, as well as the resistivity (gray; ohm-meter (ohm-m)) and sonic (turquoise; meters/second (m/s)) logs for MW35. The solid, black line on the profiles is the 3,500-m/s contour. The downline distances of the seismic profiles are relative to the positions of the respective direct-current resistivity profiles. (NAVD 88, North American Vertical Datum of 1988.)

Figure 16 shows our interpretations of lithologic boundaries along the upland profiles based on extrapolating the information from the geophysical and soil boring logs to the features and transitions observed on the geophysical profiles. These interpretations are our best explanations, albeit non-unique, for the observations in this geologically complicated area.

For Line 3 (closest to the source area), MW33 is the closest well that is located at approximately the same elevation. The MW33 lithology log shows the top of competent limestone at about 132 m elevation, corresponding with the purple 2,300- to 2,500-m/s contour of the seismic refraction velocities (fig. 14) and with the orange-red 600-ohm-m contour in the DC resistivity profile (fig. 11). The lower natural gamma log counts suggest weathered limestone between about 133-m and 135-m elevation (closely matching the lithology log) and suggest a more competent limestone below about 131 m elevation, which again matches the lithology log. There is a discrepancy, however, between the lithology and gamma logs and the seismic depth to competent bedrock. This discrepancy may be due to a complicated bedrock surface in this area as displayed by the Line 3 seismic and resistivity data and to the several meter offset between this line and MW33. The correlations between the lithology and natural gamma logs of MW21 and the seismic and resistivity data for Line 4 are very similar to those at MW33 along Line 3 but with a well-correlating competent bedrock contact.

Again, along Line 1, there is a relatively large discrepancy of about 8–10 m among our interpreted lithologic boundaries and the indication of weathered limestone in the available natural gamma log (lower counts), induction log (higher resistivity), and lithology logs from the four monitoring wells along this line. Because the limestone surface in this area changes quickly, the fact that the four wells are not located on Line 1 but about 10 m south of it might partially explain this discrepancy. It may also be due to different generations of monitoring wells that were logged by different geologists. All four wells near Line 1 were logged by the same geologist; its logs, therefore, may exhibit a more consistent bias of what is interpreted to be competent limestone, as compared to logs of MW21 and MW33 that were taken by different observers.

Interpreted Preferential Flow Paths

Line 3 exhibits interesting characteristics across the regolith/limestone contact, as determined using seismic refraction (fig. 14). The middle half of the profile exhibits a limestone high that is asymmetrically flanked on either side by what is interpreted to be a thick zone (up to 5 m) of highly fractured or weathered limestone. This feature is not seen in the resistivity profile (fig. 11) because its coverage at depth is less extensive than that for the seismic data. This limestone high and flanking regolith lows are areas of interest in terms of possible horizontal and vertical preferential flow paths for the DNAPL contaminants migrating downgradient from the source area on the limestone surface. In addition, on Lines 3 and 4 there are high gamma counts that suggest there may be thin clay lenses, which are not apparent in the resistivity profiles, separating the weathered limestone from competent bedrock, a feature that may also constrain contaminant transport.

Figure 17 shows the DC resistivity and seismic profiles in 3D space to better demonstrate how the profiles spatially relate to one another. Based on these images and on the measured contaminant levels in the wells, possible horizontal flow paths along the limestone surface are proposed. These flow paths are based on the bedrock topography and assume that the contaminant has migrated downward to the limestone near the source zone; they are not to be interpreted as the only possible flow paths. If the contaminant can be determined to be contained on the eastern side of Line 3 near MW33, then it would appear that the contamination further downgradient should be constrained to the east of the slight bedrock high at 45 m observed on the seismic profile of Line 4 (fig. 17*A*).

Though table 3 indicates that TCE and DCE contamination is present in the wells in the upland near the geophysical lines, there is not an obvious indication in the surface geophysical data of preferential flow paths from MW33 to MW21 above the competent limestone surface. There is a high resistivity spike (maximum of 1,900 ohm-m) in the resistivity log for MW34 at 120 m elevation (figs. 9, 11, and 14). Possible explanations for the spike include the presence of a lens of fresher water or a zone of entrapped DNAPL whose downward migration has been slowed or stopped by a change in fracture patterns (for example, interconnectivity or aperture) in the limestone. Unfortunately, there is no other corroborating evidence as to the cause of this anomaly; the surface resistivity measurements cannot resolve this feature at the depth at which it is present, and the gamma log shows no change.

Evidence of Multiple Clay-Rich Layers

Criss (2001) described multiple, thin (up to 20 cm each) bentonite layers in the Decorah Limestone formation that could be a possible aquitard that might create a perched water table. Based on the MW34 soil boring log, the Decorah formation is interpreted to exist from 104.4 to 111.4 m elevation (MicroPact, 2006). In the gamma logs for MW27, MW34, and MW35 (figs. 6, 9, and 10, respectively), there is a consistent pattern of two distinct layers 2 m apart that are 2 and 5 m thick with gamma counts greater than 100. The MW35 soil boring log indicated shale at 107.1 m elevation, which correlates with the position of the thicker high gamma count layer. Based on the shale classification and the consistency of the character of these beds in the gamma logs, we have indicated them on the lithology logs for these three wells as shale (figs. 6, 9, and 10). The presence of these layers cannot be confirmed by the surface geophysical data because of the limited resolving ability of such thin layers by these methods at these large depths.

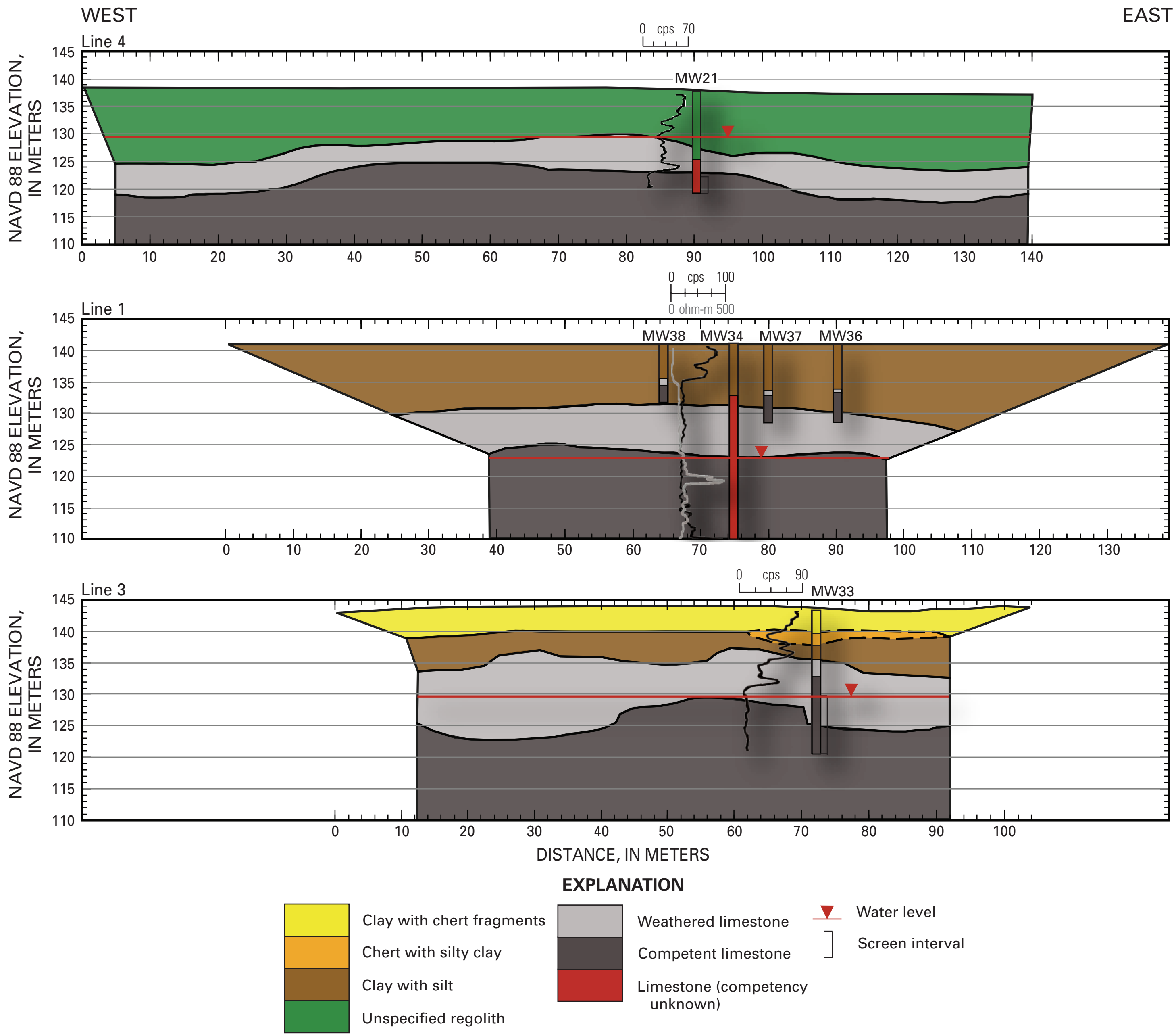

Figure 16. Integrated interpretations along the three upland surface geophysical profiles. The dashed lines indicate uncertain contacts inferred from the boreholes. The natural gamma logs (black; counts/second (cps)) are shown for MW21, MW33, and MW34, as well as the resistivity log (gray; ohm-meter (ohm-m)) for MW34. (NAVD 88, North American Vertical Datum of 1988.)

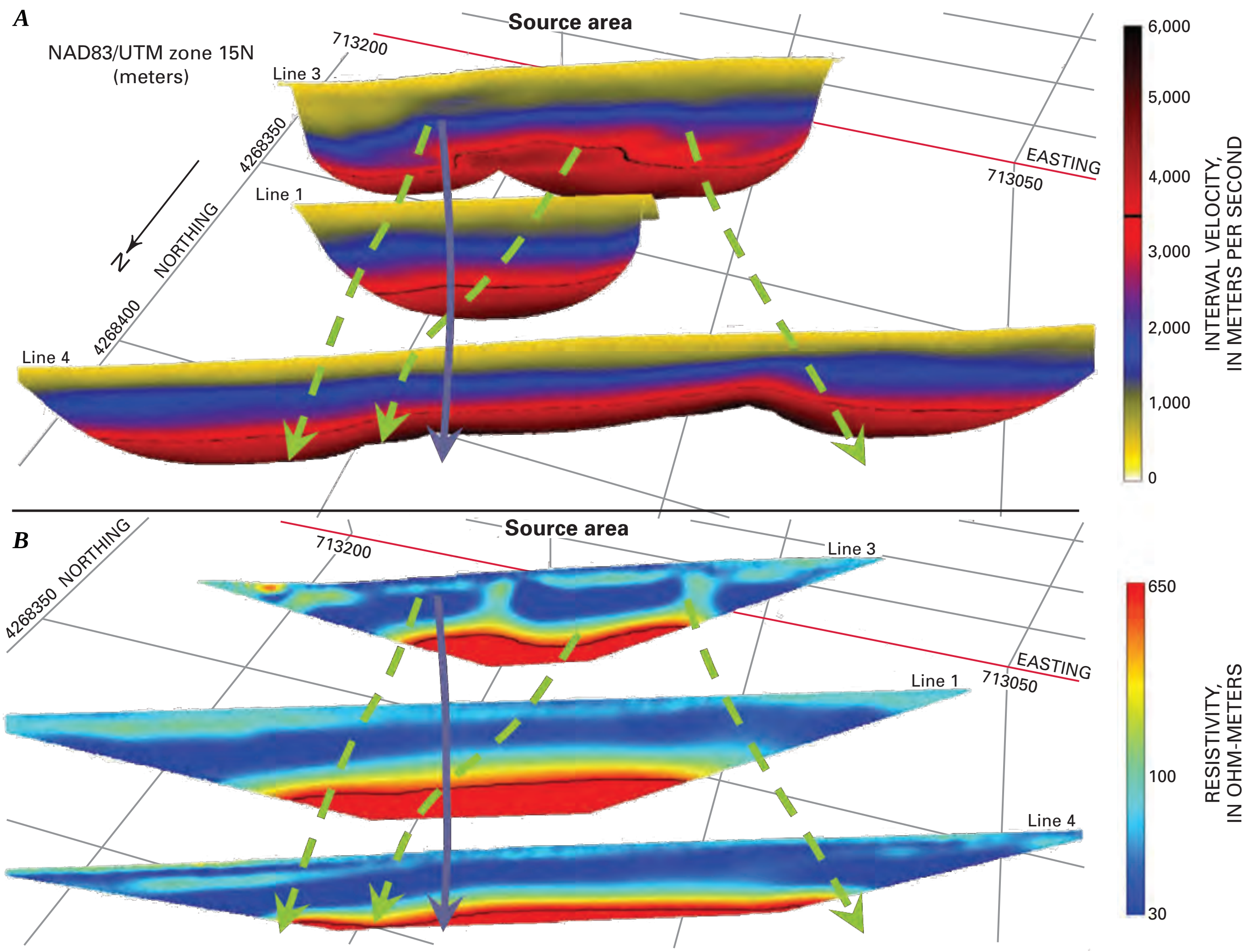

Figure 17. Oblique view toward the southeast of (*A*) seismic refraction and (*B*) direct-current resistivity profiles showing potential contaminant flow paths for the upland site based on interpreted bedrock topography. The 3,500-m/s and 650-ohm-m contours are shown in black on the seismic and resistivity profiles, respectively. The solid blue arrow indicates the most direct flow path that correlates with the three contaminated monitoring wells, and the dashed green arrows indicate other possible flow paths based on interpreted limestone topography. (NAD 83, North American Datum of 1983.)

Spikes of relatively higher gamma counts are observed at higher elevations, suggesting thin clay layers are present in the regolith and just above the weathered limestone as well. Relatively low gamma readings in the weathered and competent limestone, however, indicate generally low clay content.

Water Table Discrepancy

There is an apparent discrepancy in the elevation of the water level measured in MW34 as compared to MW21 and MW33 (see figs. 11 and 14). The lower water level in MW34 may be the potentiometric surface of a deeper aquifer in the Plattin Limestone formation into which the well is screened, from 72.1 to 76.7 m elevation (MicroPact, 2006). The bentonite layers described by Criss (2001) may be the shale layers interpreted in the gamma logs and may indeed be acting as an aquitard. In any case, it is not apparent in the geophysical data how these water table measurements might affect DNAPL transport.

Induction Log and Direct-Current Resistivity Data Discrepancy

Resistivity values determined from the induction logs in MW34 (Line 1) are similar to, but generally lower than, the values in the Line 1 DC resistivity profile. The same is true for the MW35 induction log near Line 5 of the floodplain site. This discrepancy probably is due to the presence of highly conductive bentonite cement grout that was used in all monitoring well construction at AOC 2 (MicroPact, 2006). This apparent discrepancy may also be attributed to the difference in how these two methods measure resistivity (for example, Reynolds, 1997). In addition, the surface DC resistivity method samples a much larger volume of the subsurface and therefore has a much greater averaging effect, whereas the resistivity determined from the borehole induction log measures a more localized volume directly surrounding the borehole. The relative values from the borehole induction logs, however, are still useful for interpreting relative changes and correlating them with the surface geophysical data.

Floodplain Site

The floodplain site can be broadly defined as having the following lithologies:

1. alluvium near the surface, about 7 to 15 m thick, mostly clay and sand with about an 8-m-thick gravel layer that is only present along Line 2;
2. weathered limestone bedrock, which is often identified as bedrock in the lithology logs, about 3 to 8 m thick; and
3. competent limestone bedrock, the surface of which is usually lower than the bedrock surface identified in the lithology logs.

The lithologies identified for the floodplain site are similar to those identified for the upland site except for the presence of coarser-grained alluvial deposits that do not exist on the upland site. Our interpretations of the lithologic boundaries along the floodplain profiles are shown in figure 18. The soil boring log for MW35 (figs. 10, 12, and 15) indicates that the limestone is overlain by sand and gravelly sand layers. The gamma log, however, indicates the top 3 m contains a large amount of clay, and the soil boring log for MW26, located about 10 m away but slightly closer to Line 5, does show the presence of a shallow silty clay layer. The MW26 soil boring log correlates well with the surface resistivity data, which shows a conductive layer at the surface that becomes slightly more resistive where the sand layer begins (fig. 12). The alluvium/limestone contact is well-defined in the surface resistivity data for Lines 5 and 6 and correlates well with all borehole log data from MW35 and the lithology logs from MW26 and MW35. Beginning at 150 m on Line 6, the alluvium thickens toward the east.

The gamma and soil boring logs of both MW27 and MW29, shown on Line 2 (figs. 12 and 15), indicate a surface clay layer. Although the soil boring log of MW27 indicates a 6-m-thick clay layer, the gamma log shows that it is probably only about 3 m thick, more like that shown for MW29, with an underlying layer with an increasingly lower clay content with depth. A 7- to 9-m-thick gravel layer that has not been observed elsewhere is also indicated on both soil boring logs; its position correlates well with a strong resistive layer greater than 1,300 ohm-m. The alluvium/bedrock contact is at 112 m for both wells, which also correlates well with the bottom of the resistor in the DC resistivity data. This contact correlates with a velocity of about 1,500 m/s in the seismic data. The 3,500-m/s contour is 6 m deeper and exhibits a relatively flat character across most of the profile except for a relatively strong 3-m depression centered at 415 m. Although there are lateral changes in the resistivity of the limestone in the surface resistivity data, the strong resistive gravel layer inhibits our ability to make more detailed, structural interpretations within the limestone.

Interpreted Limestone Fractured Zones

The MW35 EM induction and sonic logs (figs. 10, 12, and 15) indicate an interesting feature beginning at the alluvium/limestone contact from 115 to 119 m elevation. Based on the spiky resistivity character, decreased sonic velocities, and lack of change in the gamma log, we interpret this to be a zone of strongly fractured limestone. The increase in resistivity, however, is similar in character to the high resistivity anomaly in MW34 at 120 m elevation, which could indicate another possible entrapment of DNAPL contamination.

In the area of MW35 between 170 and 195 m on DC resistivity Line 5 (fig. 12), there is a distinct decrease in resistivity that continues to the maximum depth of the section. A similar feature is observed on Line 6 between 95 and 110 m and is interpreted to represent a wide fracture zone that may be interconnected. A similar feature along Line 2 cannot be similarly interpreted. A deepening of the bedrock velocities along the Line 5 seismic refraction profile (fig. 15) is observed at about 165 m and continues until the end of the profile but is not observed on Line 6 where the DC resistivity anomaly is present. Based on the gamma and soil boring logs, the alluvium/bedrock contact at about 119 m elevation corresponds to a velocity of only 1,200–1,300 m/s in the seismic data. The 3,500-m/s contour is about 6 m deeper (113 m elevation). The DC resistivity method appears to be more sensitive to these interpreted fracture features than seismic refraction at this site. Based on the interpretation of these more conductive features in the limestone as a fractured zone, additional possible fractures on Lines 5 and 6 (fig. 18) have been identified from the resistivity profiles; these fractures correlate with the bedrock depressions in the undulating alluvium/limestone contact in the resistivity data. Neither the dominant strike of the fracture zones nor their extensiveness can be determined from the data.

Evidence of Multiple Clay-Rich Layers

The confirmed presence of these shale, or bentonite (see Criss, 2001), layers within the Decorah Limestone may be acting to confine the underlying Plattin Limestone from the overlying regolith, alluvium, and Kimmswick Limestone. The discrepancies in the measured water levels in the upland wells support this interpretation. Although the deep placement of the screens in the floodplain wells makes it difficult to conclusively extrapolate this confinement to the floodplain site, the presence of the set of shale beds in MW27 and MW35 aids in the argument for confinement. We cannot, however, conclusively state that these layers are continuous throughout AOC 2 based on their presence in three monitoring wells. These particular layers lay at a great enough depth that the surface geophysical methods cannot resolve them. The continuity of the confining shale layers is quite important for defining the depths to which the DNAPL contaminants can vertically migrate. Although the 3,500-m/s contour lies above the shale layers in all of the floodplain profiles, the veracity of these velocities is uncertain because the interpretations of fracture zones extend to the full section depths. The interpretations on figure 18 therefore include competent bedrock contacts that

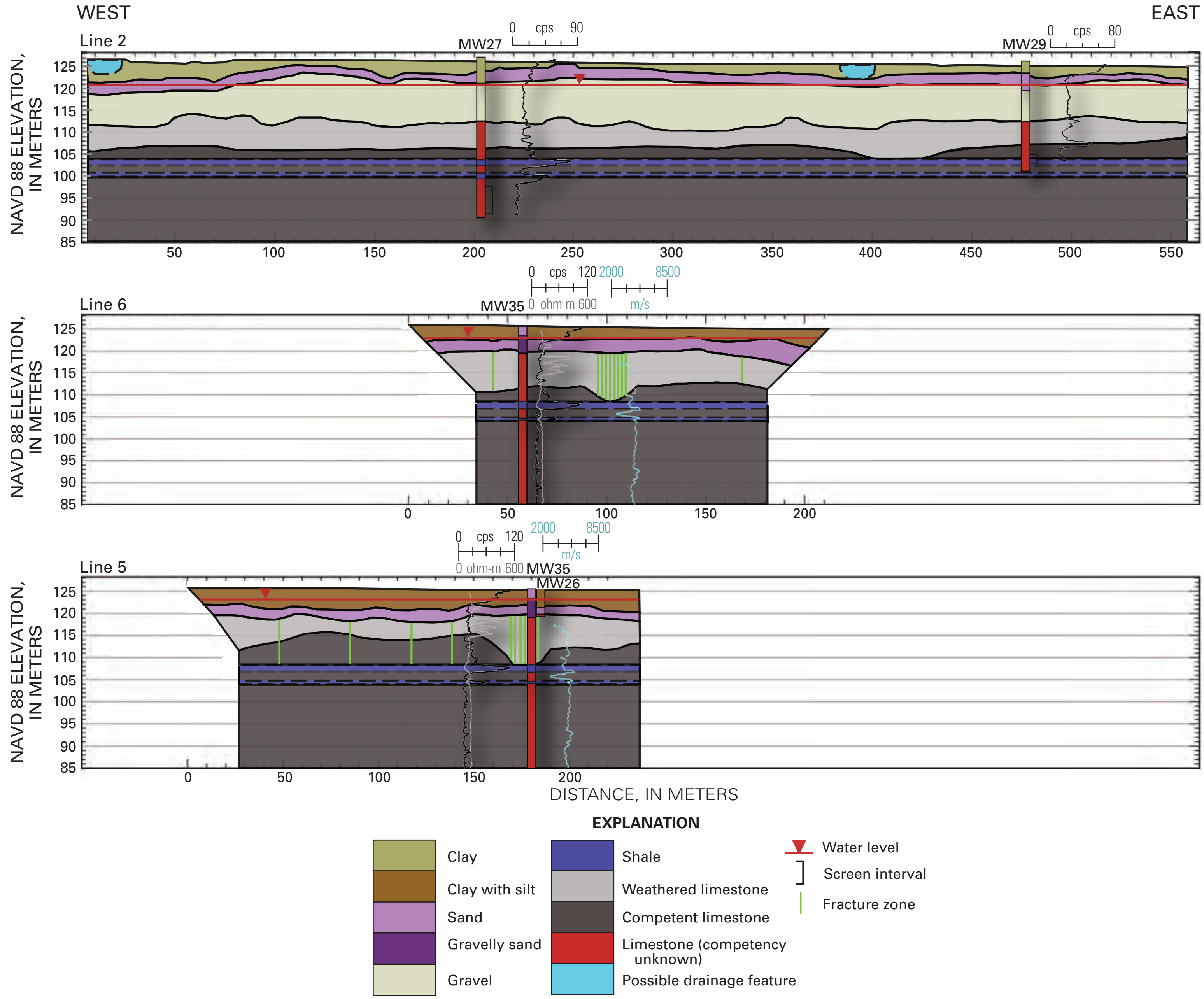

Figure 18. Integrated interpretations along the three floodplain surface geophysical profiles. The dashed lines indicate uncertain contacts inferred from the boreholes. The natural gamma logs (black; counts/second (cps)) are shown for MW27, MW29, and MW35, as well as the resistivity (gray; ohm-meter (ohm-m)) and sonic (turquoise; meters/second (m/s)) logs for MW35. (NAVD 88, North American Vertical Datum of 1988.)

are dominated by the 3,500-m/s contour but have been altered based on the DC resistivity data, with the possible extensions of the fracture zones below the weathered/competent bedrock contact presented.

In addition to the presence of the pair of shale beds in MW27, MW34, and MW35, the gamma logs indicate the presence of other, discontinuous shale-rich layers across the site (MW23 at 112 m and 108.5 m elevation, fig. 5; MW29 at 112 m elevation, fig. 7). The ability of these layers to confine is unknown. Based on the gamma logs, MW23, MW27, MW34, and MW35 have all had their screens placed beneath at least one shale-rich layer. The water levels measured may therefore be representative of lower, possibly confined aquifers and not necessarily of the Meramec River alluvium.

Summary and Conclusions

The main objective of this project was to define the occurrence and trend of possible preferential flow paths between the contaminant source area of the former TVPF AOC 2 and the Meramec River to the north. The surface geophysical data provide a more detailed, continuous image of the subsurface than what monitoring wells alone can provide. The geophysical borehole logs were a critical component in guiding our interpretations of, and in correlating the lithology logs with, the surface data as well as in delineating thin layers at depth that could not be resolved by surface methods. Potential horizontal pathways and lateral limitations of DNAPL transport were identified based on the interpreted limestone bedrock topography in the upland site. We also identified possible vertical fracture zones in the southern part of the floodplain that could be major routes for ground water flow toward the Meramec River. The presence of multiple confining shale layers in the Decorah formation are important in defining possible obstacles to the downward migration of DNAPL contaminants. Unfortunately, surface geophysical methods cannot resolve these relatively thin layers at the depths at which they are present; only borehole logs, specifically gamma and EM induction logs, are capable of locating the clay-rich layers.

The contaminant source area is located over a complicated section of limestone bedrock. In Line 3, which is closest to the source area, we interpret a bedrock high that is flanked on both sides by large sections of weathered/fractured limestone as a possible horizontal and vertical preferential flow path. Both the surface resistivity and seismic refraction sections exhibit complicated patterns that are not fully understood. To more conclusively constrain possible flow paths emanating from the source area, however, more detail of the limestone surface directly below the source area is required.

The multi-disciplinary approach using seismic refraction and DC resistivity surface methods yields a more confident interpretation than that obtained using only a single method. The use of available well construction reports and lithologic logs is imperative to interpreting the geophysical results. It is particularly important for a study involving ground water flow and contaminant transport to carefully study the lithologic logs in terms of the noted degree of weathering and fracturing of the bedrock. The presence of bedrock in lithologic logs alone does not imply the existence of truly competent, hard rock that could influence ground water flow. By using both surface and borehole geophysics to help determine a competent bedrock contact or thin, potentially confining beds, more effective monitoring and remediation strategies can be established.

Acknowledgments

This work was funded by the USACE Kansas City District under interagency agreement W58XUW61171975 and W58XUW70332441. We would like to acknowledge Mirek Towster of the USACE Kansas City District for funding the geophysical data collection; Bill Ferguson of the USACE Kansas City District for his assistance during data acquisition and support during data processing and interpretation; David Back of MicroPact Engineering for assisting in the borehole logging data acquisition and for providing monitoring well information from the site; and Justin Davis, Douglas Mugel, and Paul Rydlund of the USGS Missouri Water Science Center for assisting in field operations. We also appreciate the thorough technical reviews by Jeff Lucius and Mike Powers of the USGS Crustal Imaging and Characterization Team that helped to make this a better report.

References Cited

Advanced Logic Technologies, 2004, WellCAD for Win 32™: Advanced Logic Technology, Batiment A, Route de Niederpallen, L-8506 Redange-sur-Attert, Luxembourg.

American Society for Testing and Materials, 2001, Standard guide for conducting borehole geophysical logging—Electromagnetic induction: American Society for Testing and Materials standard D 6726–01, 7 p.

American Society for Testing and Materials, 2004, Standard guide for conducting borehole geophysical logging—Gamma: American Society for Testing and Materials standard D 6274–98, 11 p.

Ball, L.B., Kress, W.H., Anderson, E.D., Teeple, A.P., Ferguson, J.W., and Colbert, C.R., 2004, Surface geophysical investigation of the areal and vertical extent of metallic waste at the former Tyson Valley Powder Farm near Eureka, Missouri, spring 2004: U.S. Geological Survey Scientific Investigations Report 2004–5208, 66 p.

Benham, K.E., 1982, Soil survey of St. Louis County and St. Louis City, Missouri: U.S. Department of Agriculture, Soil Conservation Service.

Butler, D.K, ed., 2005, Near-surface geophysics: Tulsa, Okla., Society of Exploration Geophysicists Investigations in Geophysics no. 13, 732 p.

Criss, R.E., 2001, Hydrogeology of Tyson Research Center, Lone Elk County Park, and West Tyson County Park, eastern Missouri: U.S. Environmental Protection Agency Region 7, 58 p., *http://www.biology.wustl.edu/tyson/geology.html*, September 2007.

Encom, 2004, Profile Analyst user's manual: Milsons Point, Australia, Encom, Inc.

Gebrande, H., and Miller, H., 1985, Refraktionsseismik, *in* Bender, Friedrich, ed., Angewandte Geowissenschaften: Stuttgart, Germany, Ferdinand Enke Verlag.

Imes, J.L., and Emmett, L.F., 1994, Geohydrology of the Ozark Plateau aquifer system in parts of Missouri, Arkansas, Oklahoma, and Kansas: U.S. Geological Survey Professional Paper 1414–D, 127 p.

Intelligent Resources Inc., 2006, Rayfract manual—Tutorial: Vancouver, B.C., Canada, Intelligent Resources, Inc., 18 p., *http://rayfract.com/help/manual.pdf*, 27 August 2007.

Intelligent Resources Inc., 2007, Rayfract seismic refraction tomography: Intelligent Resources, Inc., *http://www.rayfract.com*, 17 September 2007.

Keys, W.S., 1990, Borehole geophysics applied to ground-water investigations: U.S. Geological Survey Techniques of Water-Resource Investigation 02–E2, 150 p.

Keys, W.S., 1997, A practical guide to borehole geophysics in environmental investigations: Boca Raton, Fla., CRC-Lewis Publishers, 176 p.

Kring, D., and Bailey, D., 2001, Tyson Valley (ex.) Army powder storage farm, St. Louis, Missouri: U.S. Environmental Protection Agency Region 7 Fact Sheet, 2 p.

Larson, David, 2007, Precipitation at Tyson Research Center, near Eureka, St. Louis County, Missouri, 1977 to present: Tyson Research Center, *http://www.biology.wustl.edu/tyson/archivesprec.html*, 27 August 2007.

Loke, M.H., 2000, Electrical imaging surveys for environmental and engineering studies—A practical guide to 2-D and 3-D surveys: Penang, Malaysia, M.H. Loke, 62 p., *http://www.geoelectrical.com*, August 2007.

Loke, M.H., 2004, RES2DINV, version 3.55—Rapid 2D resistivity and IP inversion using the least-squares method—Geoelectrical imaging 2-D and 3-D: Penang, Malaysia, Geotomo Software, 139 p., http://www.geoelectrical.com, 2 January 2007.

MicroPact, 2004, Final pilot study report—Pilot study report for soil remediation, Area of Concern 2, former Tyson Valley Powder Farm: Herndon, Virginia, MicroPact Engineering, 20 p.

MicroPact, 2006, Packet of available driller's logs, soil boring logs, construction reports, and well development records for AOC 2 monitoring wells: Herndon, Virginia, MicroPact Engineering, Inc., 139 p., received 2006.

Mount Sopris Instrument Co., 2002, 2PIA-1000 poly induction probe, 2EMA-1000 conductivity probe (2EMB-1000 and 2EMC-1000), EMP-2493 and EMP-4493 operating manual: Golden, Colo., Mount Sopris Instrument Co., Inc., 19 p.

Powers, M.H., and Burton, B.L., 2007, Questa baseline and pre-mining ground-water quality investigation. 24. Seismic refraction tomography for volume analysis of saturated alluvium in the Straight Creek drainage and its confluence with Red River, Taos County, New Mexico: U.S. Geological Survey Scientific Investigations Report 2006–5166, 19 p.

Powers, M.H., Haines, S.S., and Burton, B.L., 2007, Compressional and shear wave seismic refraction tomography at Success Dam, Porterville, California, *in* Gamey, J., ed., Symposium on the Application of Geophysics to Engineering and Environmental Problems, Denver, Colo., 1–5 April 2007, Proceedings, 10 p.

Reynolds, J.M., 1997, An introduction to applied and environmental geophysics: Chichester, England, John Wiley and Sons, 796 p.

Schuster, G.T., and Quintus-Bosz, A., 1993, Wavepath eikonal traveltime inversion—Theory: Geophysics, v. 58, no. 9, p. 1,314–1,323.

Sharma, P.V., 1997, Environmental and engineering geophysics: Cambridge, U.K., Cambridge University Press, 475 p.

Telford, W.M., Geldart, L.P., and Sheriff, R.E., 1990, Applied geophysics (2d ed.): Cambridge, U.K., Cambridge University Press, 770 p.

U.S. Environmental Protection Agency, 2006a, Consumer factsheet on trichloroethylene: Environmental Protection Agency, Office of Ground Water and Drinking Water, *http://www.epa.gov/safewater/contaminants/dw_contamfs/trichlor.html*, 30 October 2007.

U.S. Environmental Protection Agency, 2006b, Consumer factsheet on 1,1-Dichloroethylene: Environmental Protection Agency, Office of Ground Water and Drinking Water, *http://www.epa.gov/safewater/dwh/c-voc/11-dichl.html*, 30 October 2007.

U.S. Geological Survey, 2007, USGS 07019000 Meramec River near Eureka, MO: U.S. Geological Survey National Water Information System, *http://waterdata.usgs.gov/nwis/uv/?site_no=07019000&PARAmeter_cd=00065,00060,00062,72020*, 27 August 2007.

Appendixes

Appendix 1. Geophysical Well Logs Acquired at AOC 2 Monitoring Wells

Well logs acquired in the accessible monitoring wells at the former TVPF AOC 2, May 2006. Data for all tools we used in each well are shown.

Monitoring Well 21
Monitoring Well 23
Monitoring Well 27
Monitoring Well 29
Monitoring Well 33
Monitoring Well 34
Monitoring Well 35

Click on the links above to access PDF files for each well.

Appendix 2. Summary of Raw and Calculated Pseudosections and Final Inversions of Direct-Current Resistivity Data

Inverted Wenner-Schlumberger DC resistivity profiles (bottom image) with raw data (top image) and forward modeled (middle image) pseudosections. Data acquired at AOC 2, May 2006. The color scales are different for each profile. The white dots in the two pseudosections represent the individual measured data points. For all images, the horizontal axis is downline distance, in meters, and the vertical axis is depth, in meters.

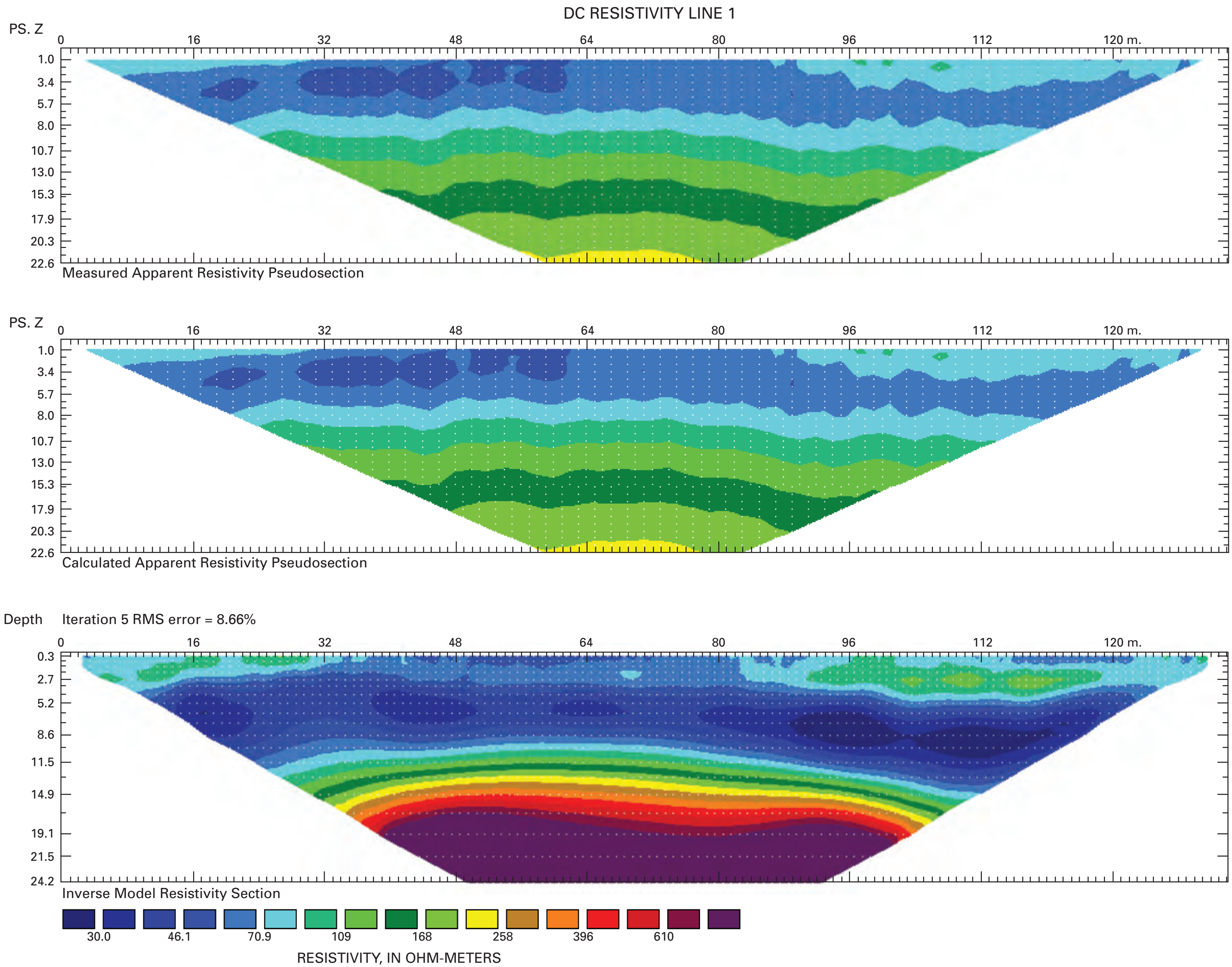
DC RESISTIVITY LINE 1
PS. Z
0 16 32 48 64 80 96 112 120 m.
1.0 3.4 5.7 8.0 10.7 13.0 15.3 17.9 20.3 22.6
Measured Apparent Resistivity Pseudosection
PS. Z
0 16 32 48 64 80 96 112 120 m.
1.0 3.4 5.7 8.0 10.7 13.0 15.3 17.9 20.3 22.6
Calculated Apparent Resistivity Pseudosection
Depth
Iteration 5 RMS error = 8.66%
0 16 32 48 64 80 96 112 120 m.
0.3 2.7 5.2 8.6 11.5 14.9 19.1 21.5 24.2
Inverse Model Resistivity Section
30.0 46.1 70.9 109 168 258 396 610
RESISTIVITY, IN OHM-METERS

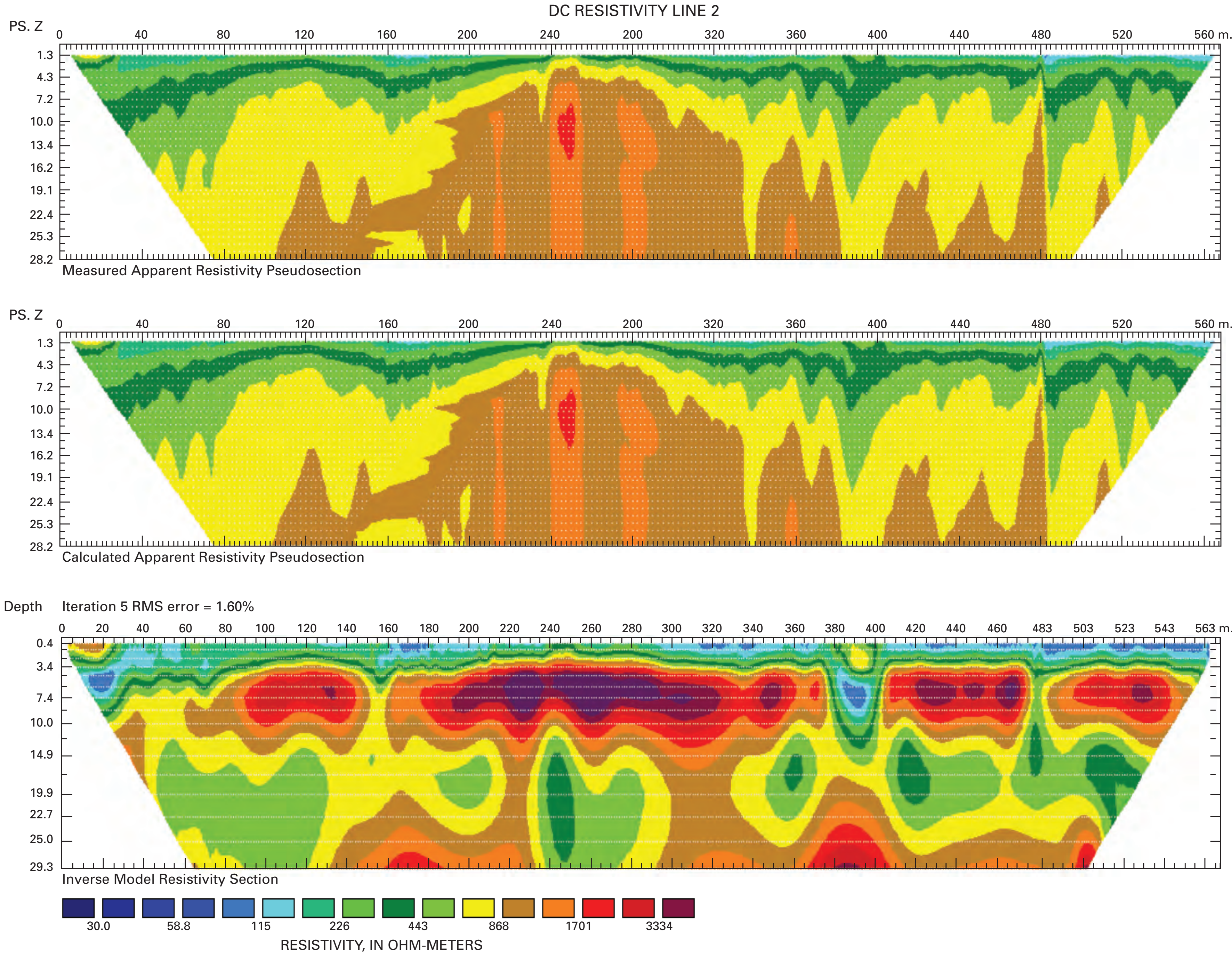
DC RESISTIVITY LINE 2
PS. Z
0 40 80 120 160 200 240 200 320 360 400 440 480 520 560 m.
1.3 4.3 7.2 10.0 13.4 16.2 19.1 22.4 25.3 28.2
Measured Apparent Resistivity Pseudosection
PS. Z
0 40 80 120 160 200 240 200 320 360 400 440 480 520 560 m.
1.3 4.3 7.2 10.0 13.4 16.2 19.1 22.4 25.3 28.2
Calculated Apparent Resistivity Pseudosection
Depth
Iteration 5 RMS error = 1.60%
0 20 40 60 80 100 120 140 160 180 200 220 240 260 280 300 320 340 360 380 400 420 440 460 483 503 523 543 563 m.
0.4 3.4 7.4 10.0 14.9 19.9 22.7 25.0 29.3
Inverse Model Resistivity Section
30.0 58.8 115 226 443 868 1701 3334
RESISTIVITY, IN OHM-METERS

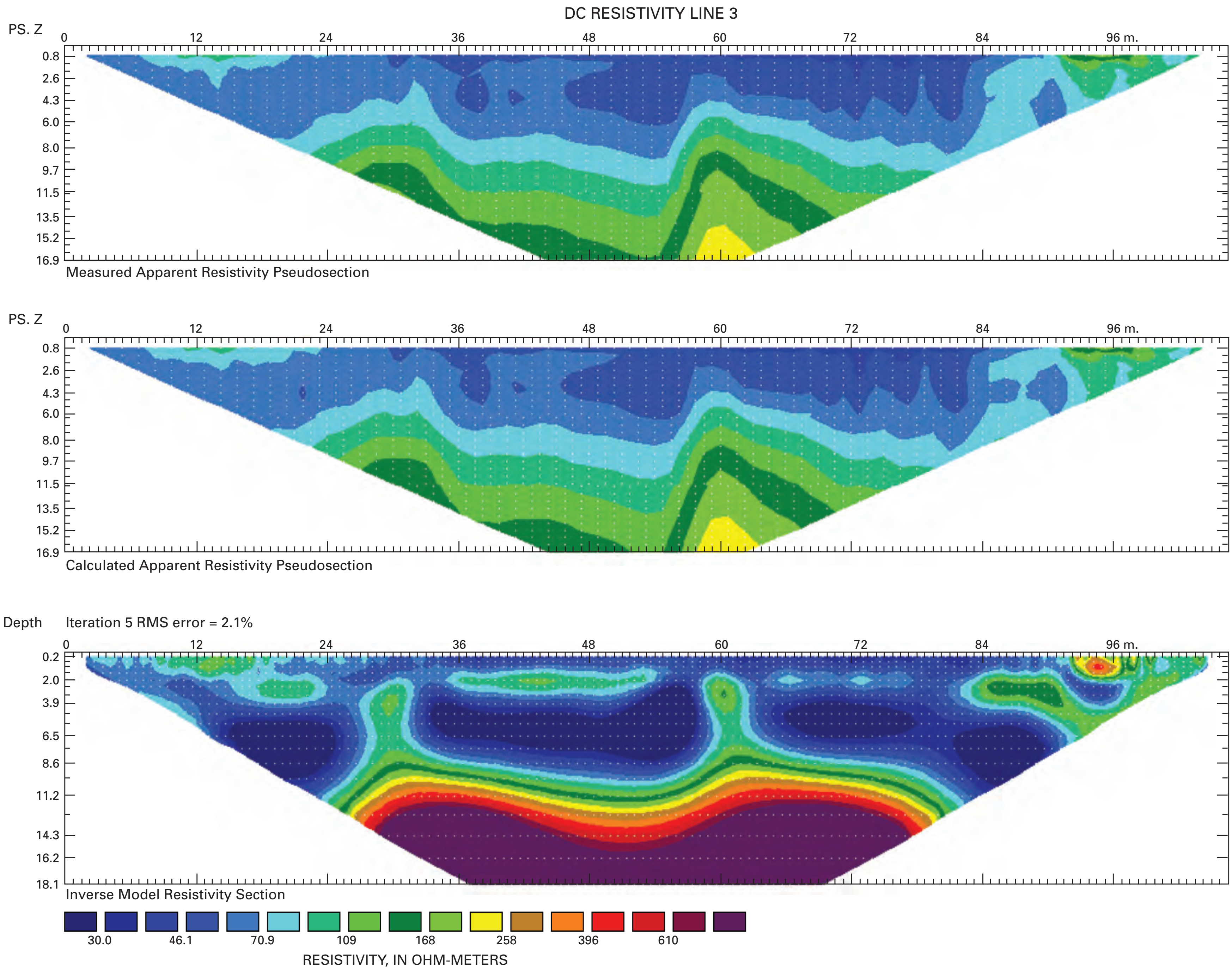
DC RESISTIVITY LINE 3
PS. Z
0 12 24 36 48 60 72 84 96 m.
0.8 2.6 4.3 6.0 8.0 9.7 11.5 13.5 15.2 16.9
Measured Apparent Resistivity Pseudosection
PS. Z
0 12 24 36 48 60 72 84 96 m.
0.8 2.6 4.3 6.0 8.0 9.7 11.5 13.5 15.2 16.9
Calculated Apparent Resistivity Pseudosection
Depth
Iteration 5 RMS error = 2.1%
0 12 24 36 48 60 72 84 96 m.
0.2 2.0 3.9 6.5 8.6 11.2 14.3 16.2 18.1
Inverse Model Resistivity Section
30.0 46.1 70.9 109 168 258 396 610
RESISTIVITY, IN OHM-METERS

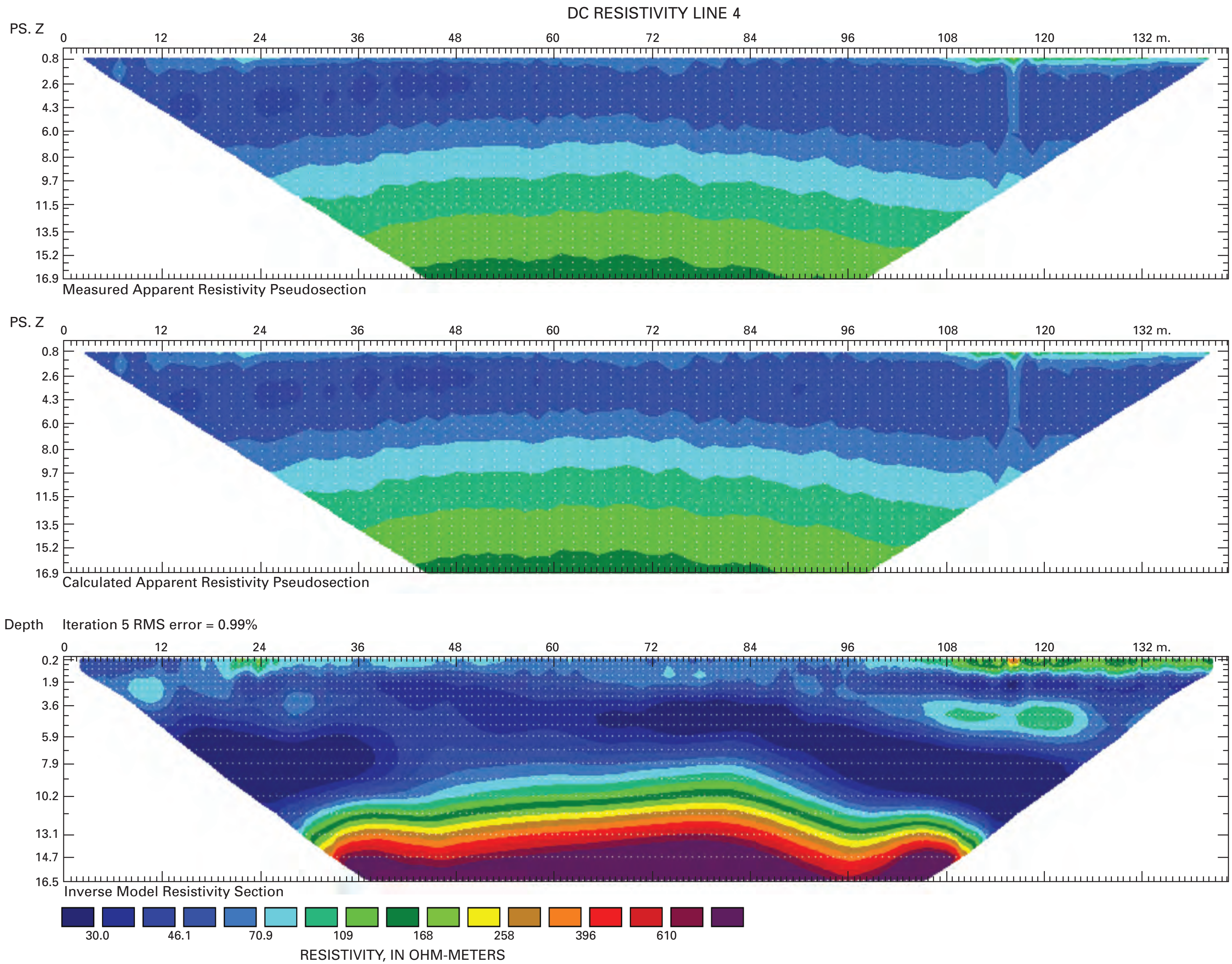
DC RESISTIVITY LINE 4
PS. Z
0 12 24 36 48 60 72 84 96 108 120 132 m.
0.8 2.6 4.3 6.0 8.0 9.7 11.5 13.5 15.2 16.9
Measured Apparent Resistivity Pseudosection
PS. Z
0 12 24 36 48 60 72 84 96 108 120 132 m.
0.8 2.6 4.3 6.0 8.0 9.7 11.5 13.5 15.2 16.9
Calculated Apparent Resistivity Pseudosection
Depth
Iteration 5 RMS error = 0.99%
0 12 24 36 48 60 72 84 96 108 120 132 m.
0.2 1.9 3.6 5.9 7.9 10.2 13.1 14.7 16.5
Inverse Model Resistivity Section
30.0 46.1 70.9 109 168 258 396 610
RESISTIVITY, IN OHM-METERS

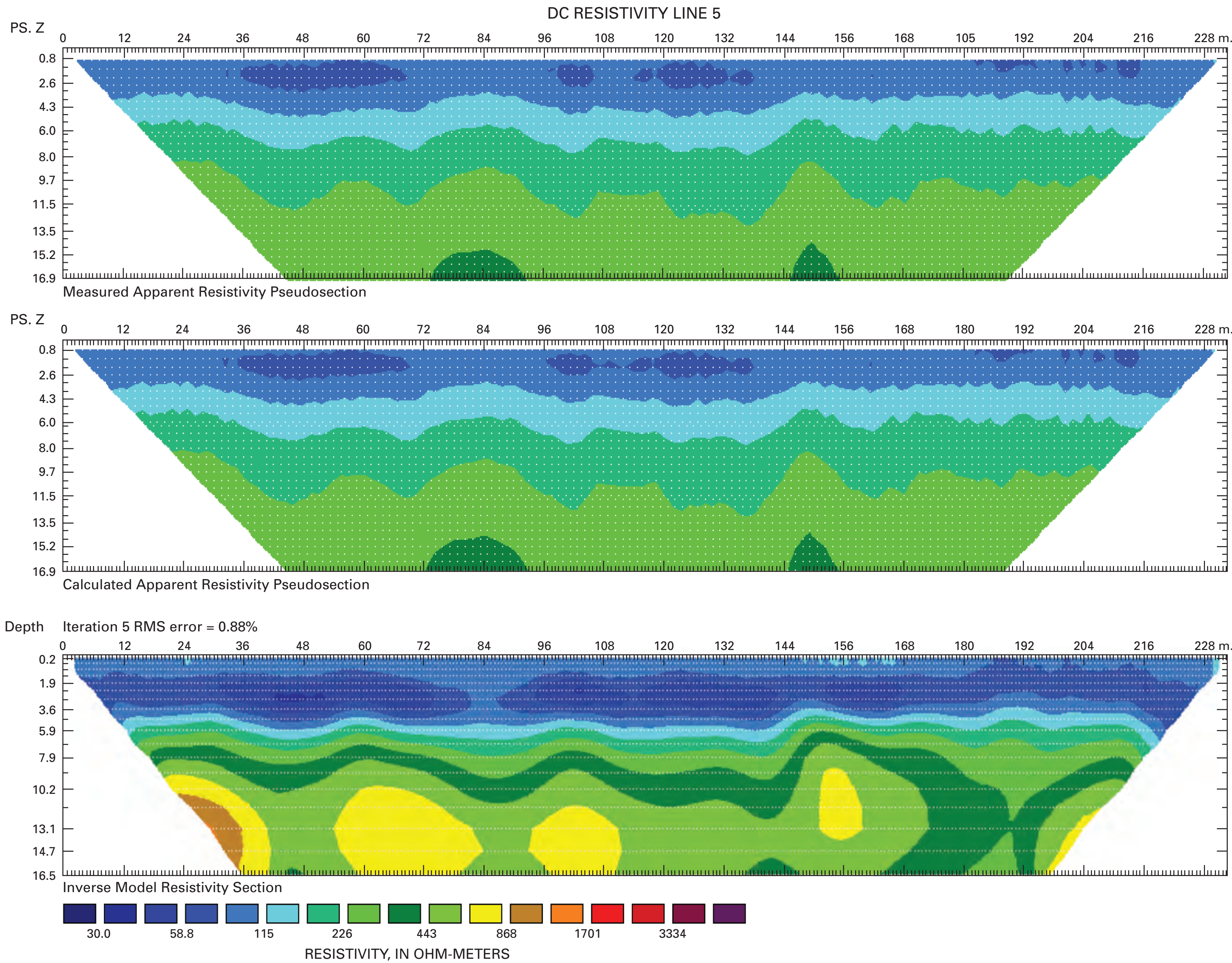
DC RESISTIVITY LINE 5
PS. Z
0 12 24 36 48 60 72 84 96 108 120 132 144 156 168 105 192 204 216 228 m.
0.8 2.6 4.3 6.0 8.0 9.7 11.5 13.5 15.2 16.9
Measured Apparent Resistivity Pseudosection
PS. Z
0 12 24 36 48 60 72 84 96 108 120 132 144 156 168 180 192 204 216 228 m.
0.8 2.6 4.3 6.0 8.0 9.7 11.5 13.5 15.2 16.9
Calculated Apparent Resistivity Pseudosection
Depth
Iteration 5 RMS error = 0.88%
0 12 24 36 48 60 72 84 96 108 120 132 144 156 168 180 192 204 216 228 m.
0.2 1.9 3.6 5.9 7.9 10.2 13.1 14.7 16.5
Inverse Model Resistivity Section
30.0 58.8 115 226 443 868 1701 3334
RESISTIVITY, IN OHM-METERS

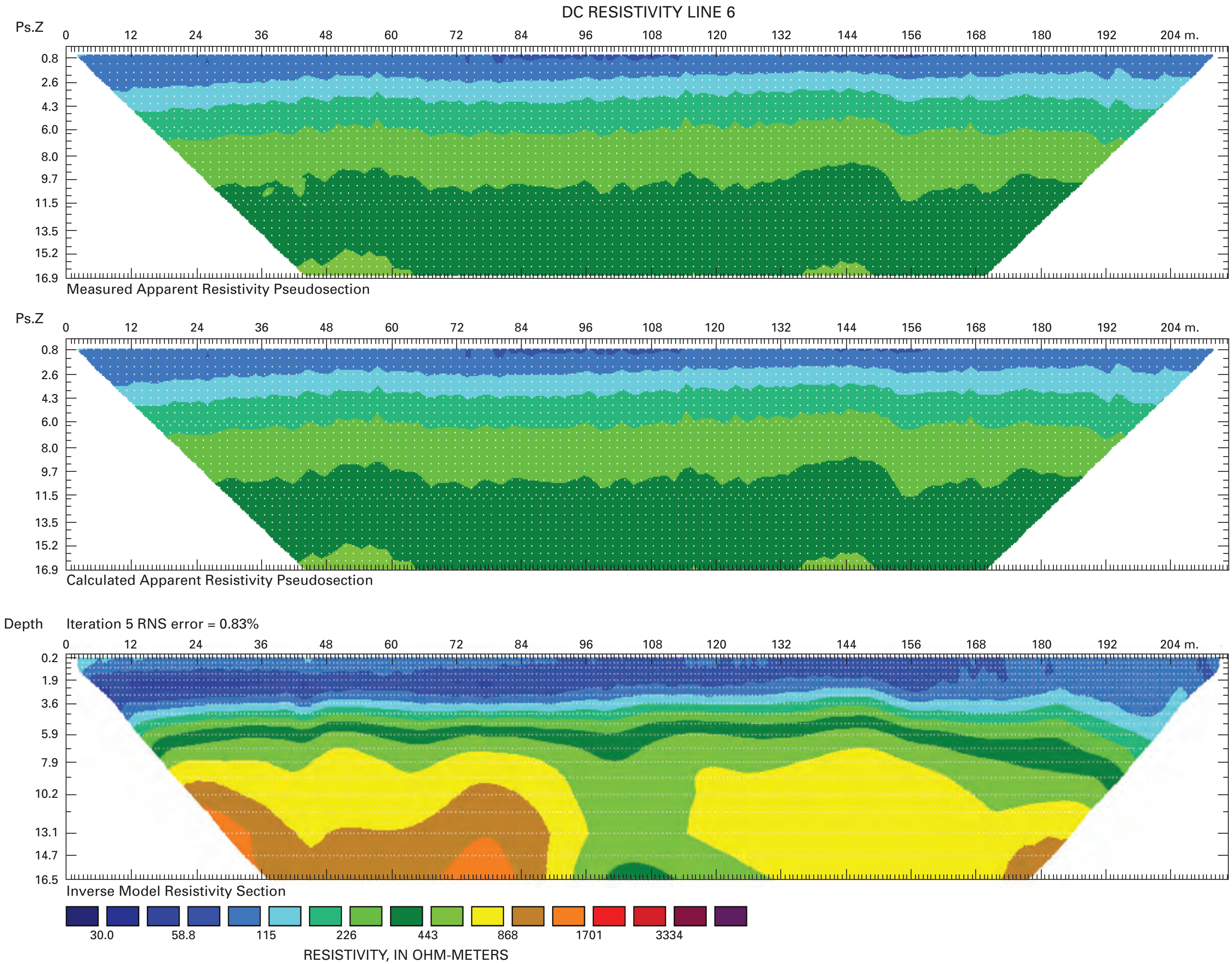
DC RESISTIVITY LINE 6
Ps.Z
0 12 24 36 48 60 72 84 96 108 120 132 144 156 168 180 192 204 m.
0.8 2.6 4.3 6.0 8.0 9.7 11.5 13.5 15.2 16.9
Measured Apparent Resistivity Pseudosection
Ps.Z
0 12 24 36 48 60 72 84 96 108 120 132 144 156 168 180 192 204 m.
0.8 2.6 4.3 6.0 8.0 9.7 11.5 13.5 15.2 16.9
Calculated Apparent Resistivity Pseudosection
Depth
Iteration 5 RNS error = 0.83%
0 12 24 36 48 60 72 84 96 108 120 132 144 156 168 180 192 204 m.
0.2 1.9 3.6 5.9 7.9 10.2 13.1 14.7 16.5
Inverse Model Resistivity Section
30.0 58.8 115 226 443 868 1701 3334
RESISTIVITY, IN OHM-METERS

Appendix 3. Raw First Break Pick and Forward Modeled Traveltime Curves of Seismic Refraction Data

Traveltime curves for each seismic refraction line. The top image is of the first break travel times, and the bottom image has the raytraced travel times overlain to show how well the model fit the data. The different colors of the traveltime curves are meaningless. The dashed line segments of the curves indicate where no first breaks were picked. Geophones were located at the positive integer station locations, and the shots were at half station intervals. Data acquired at AOC 2, May 2006.

Seismic Line 1
Station spacing = 1 m

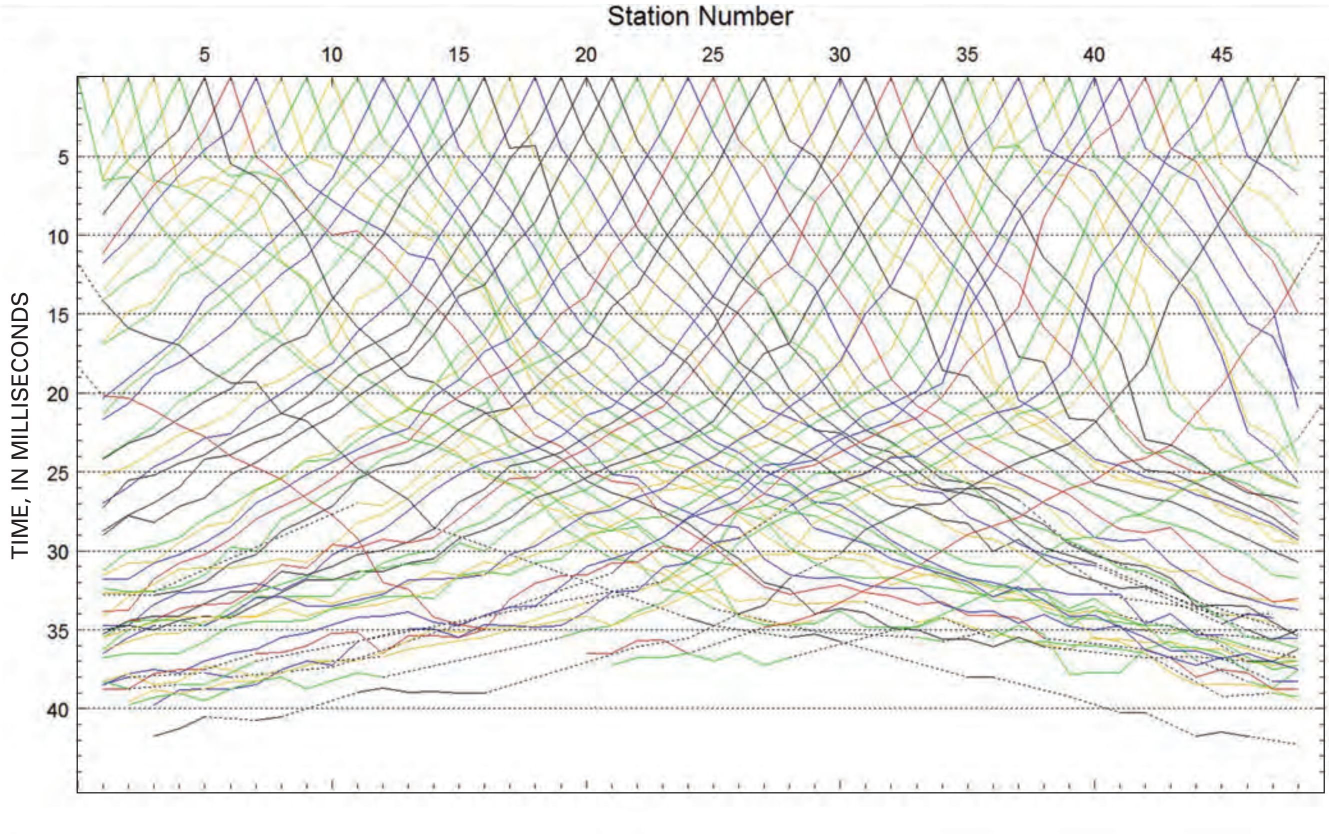

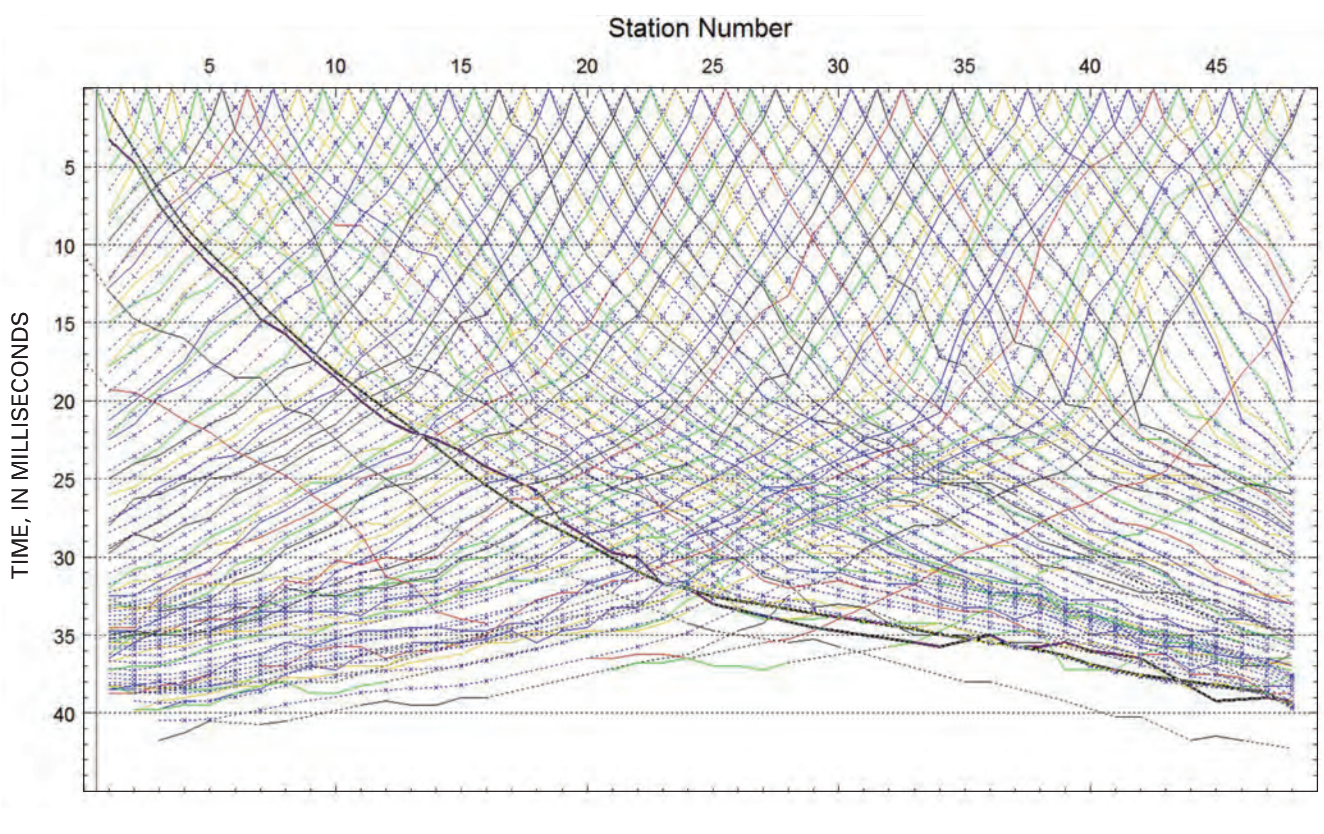

Seismic Line 2
Station spacing = 2.5 m

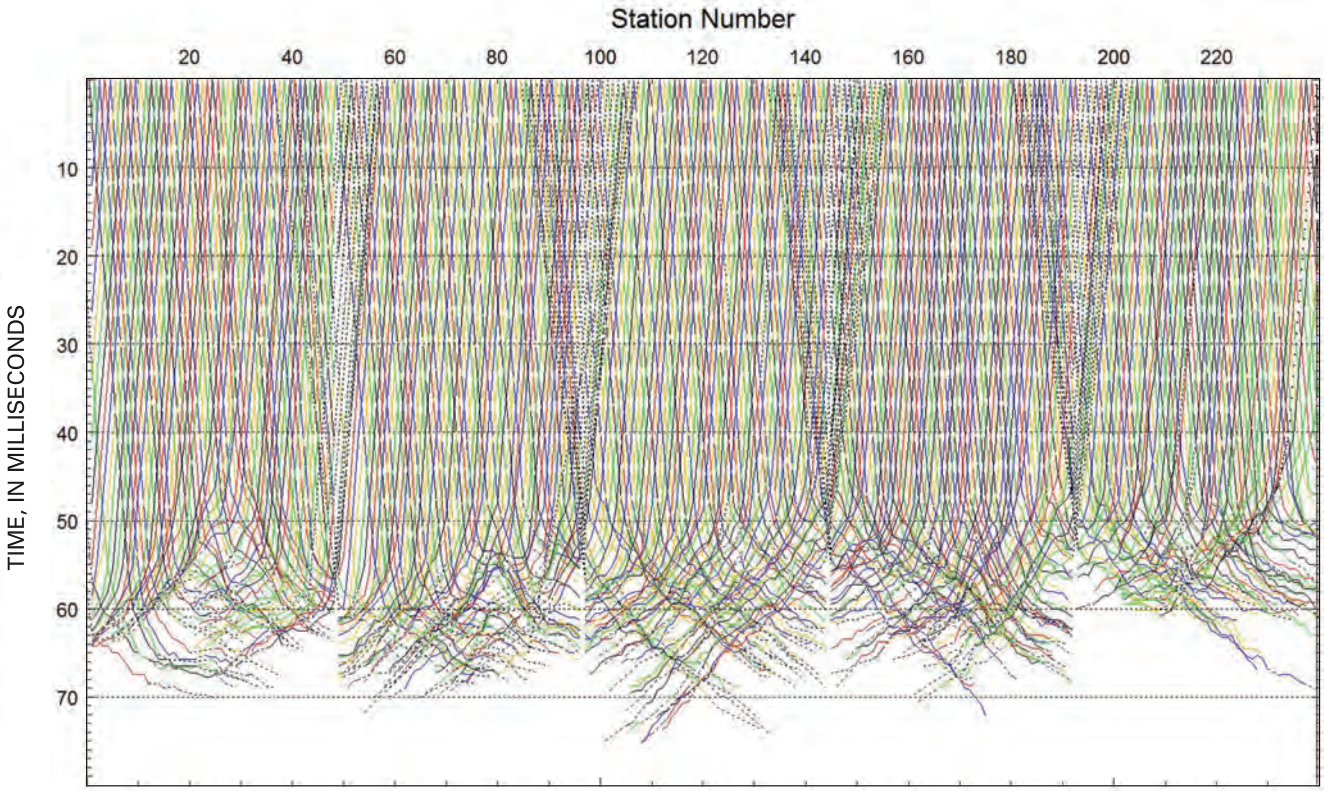

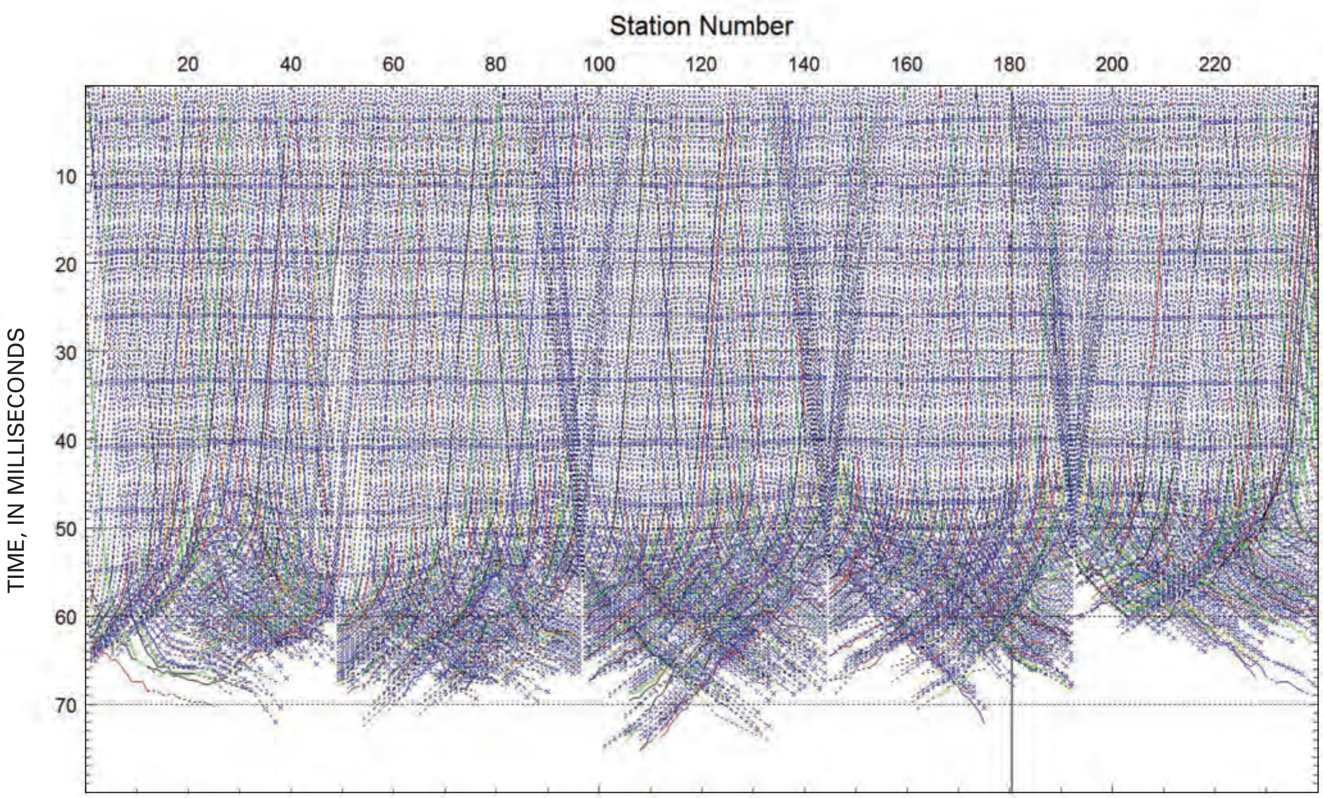

Seismic Line 3
Station spacing = 1 m

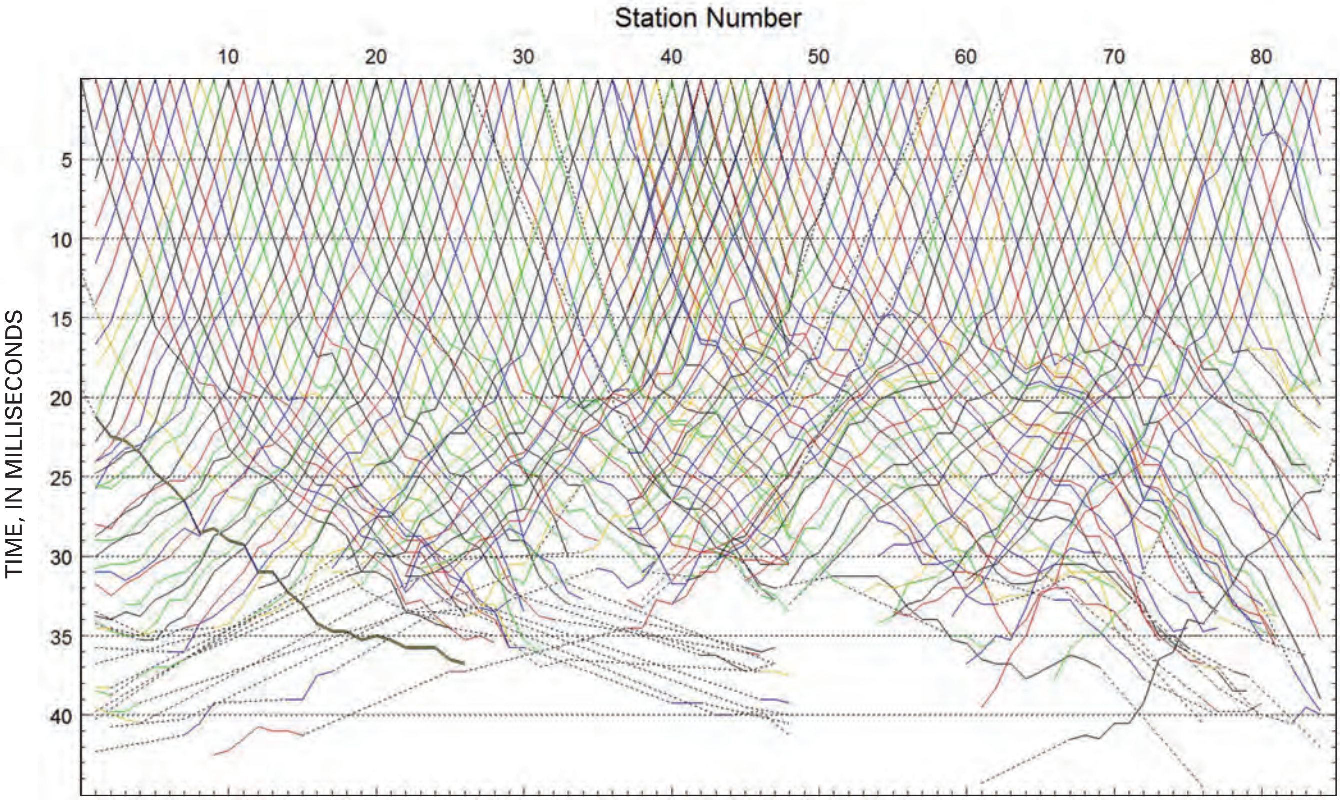

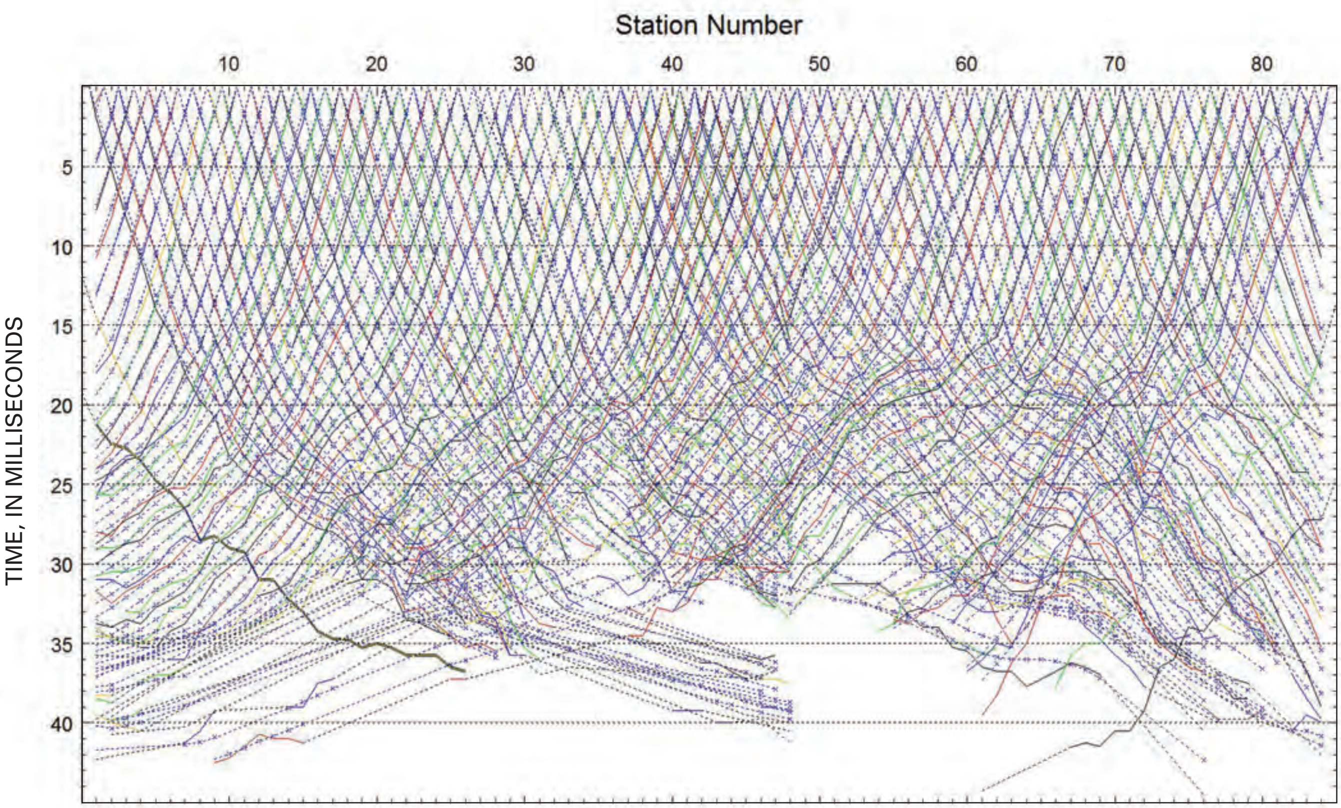

Seismic Line 4
Station spacing = 1 m

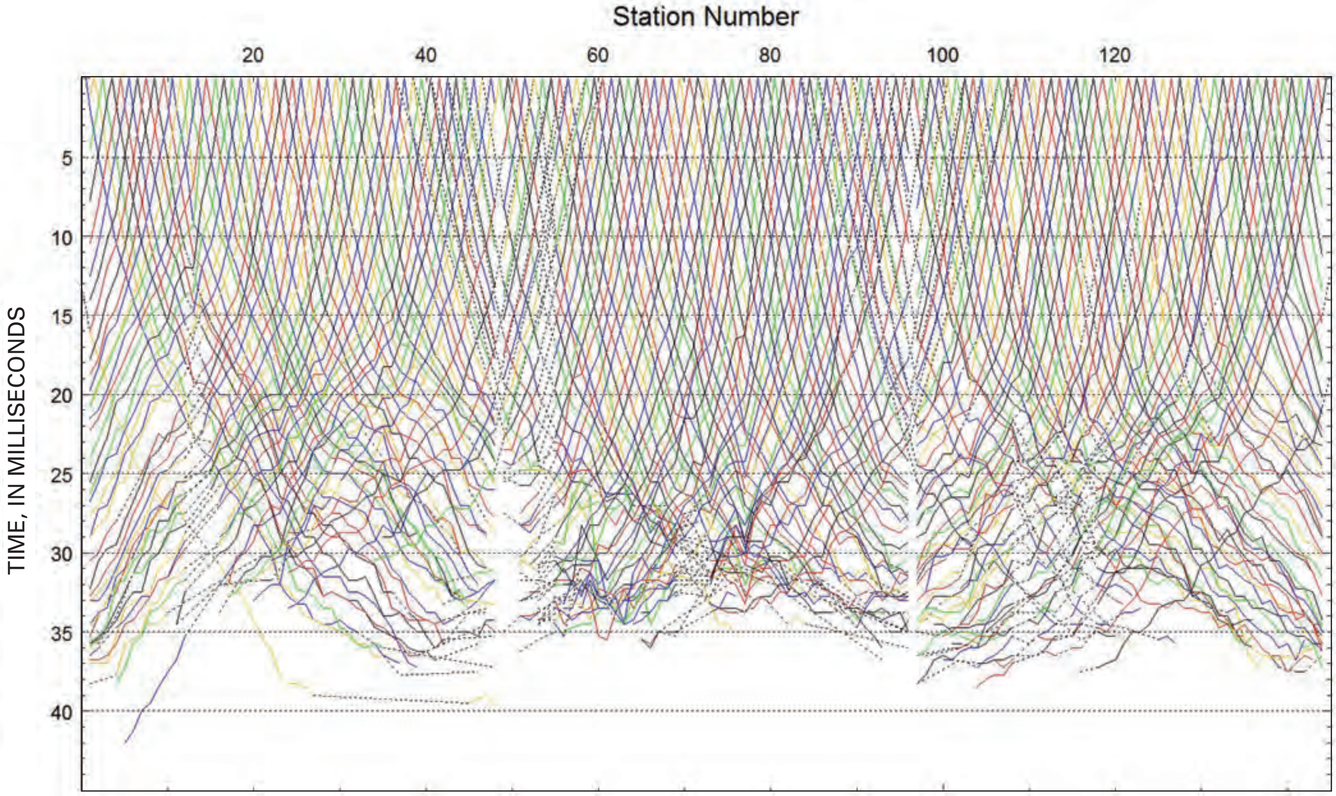

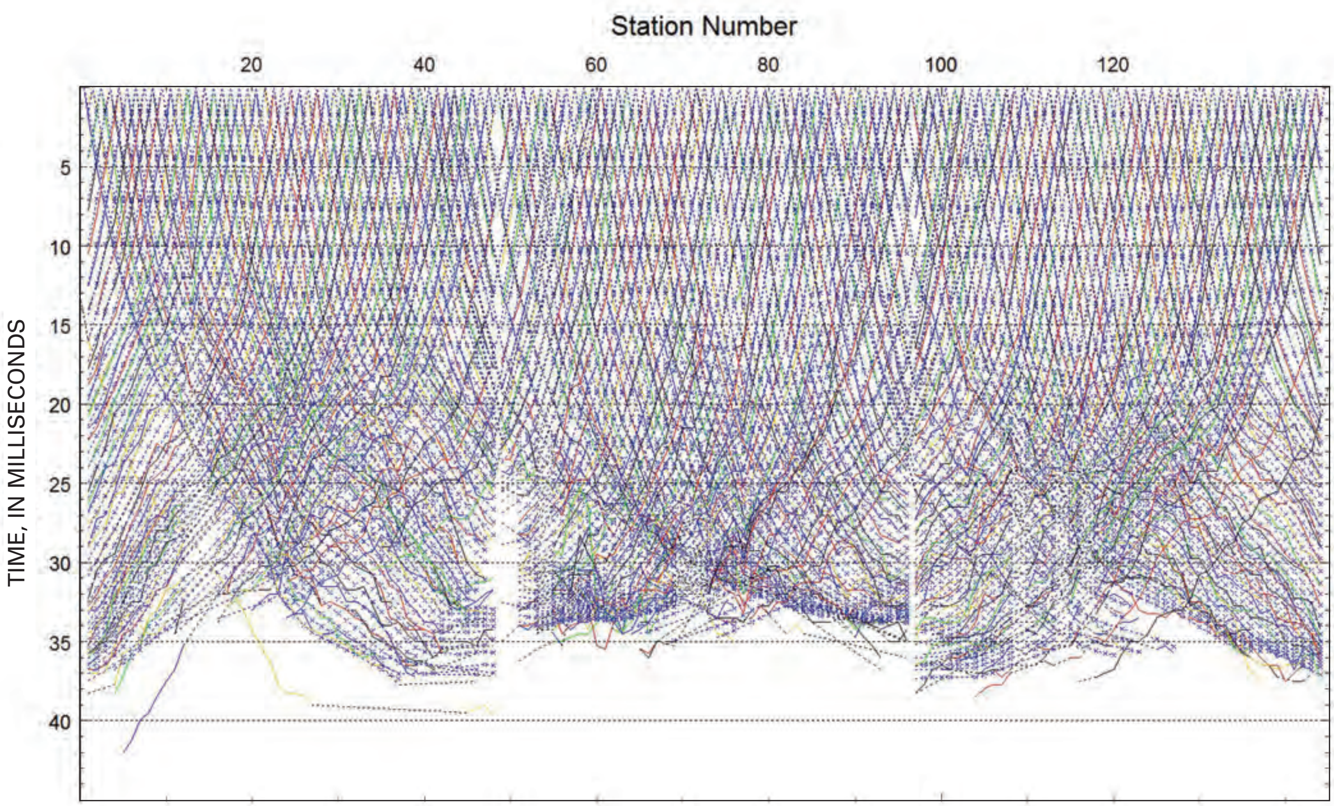

Seismic Line 5

Station spacing = 1.5 m

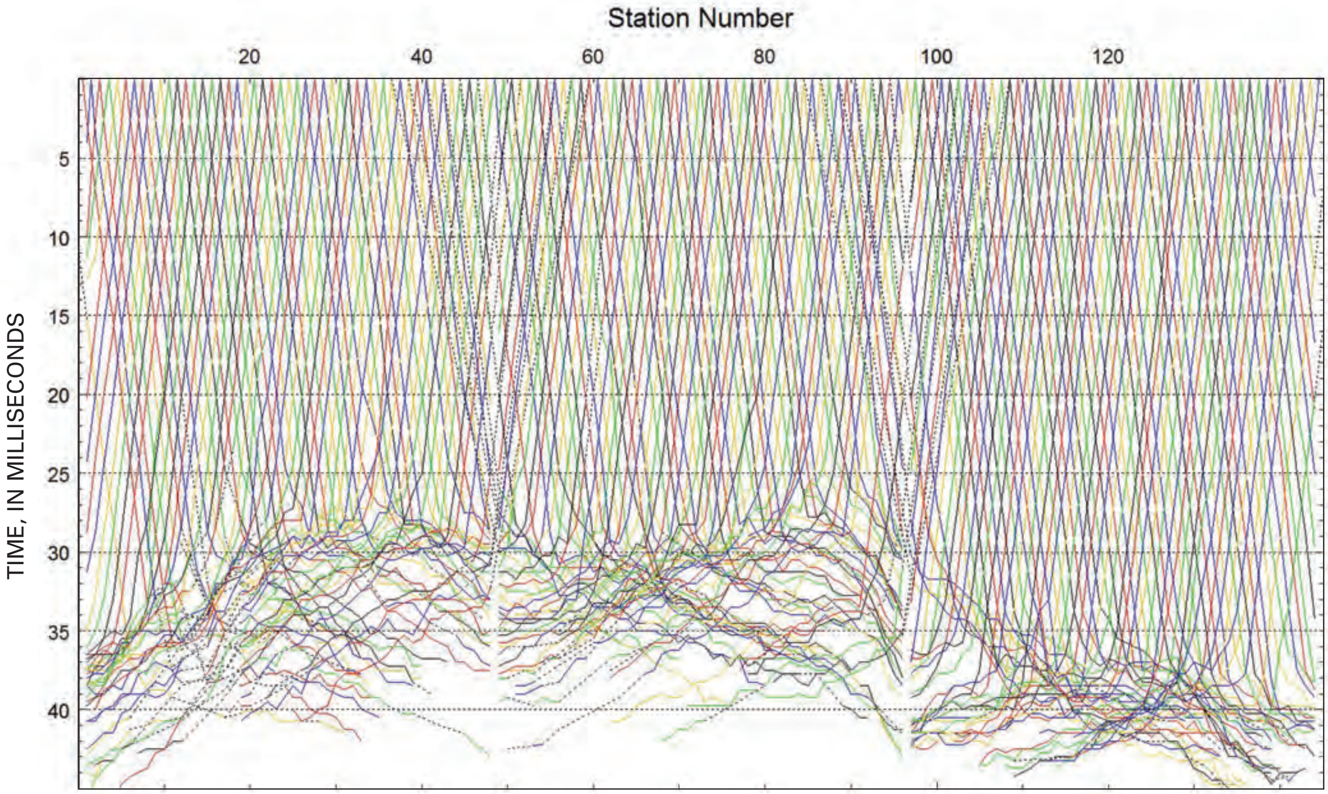

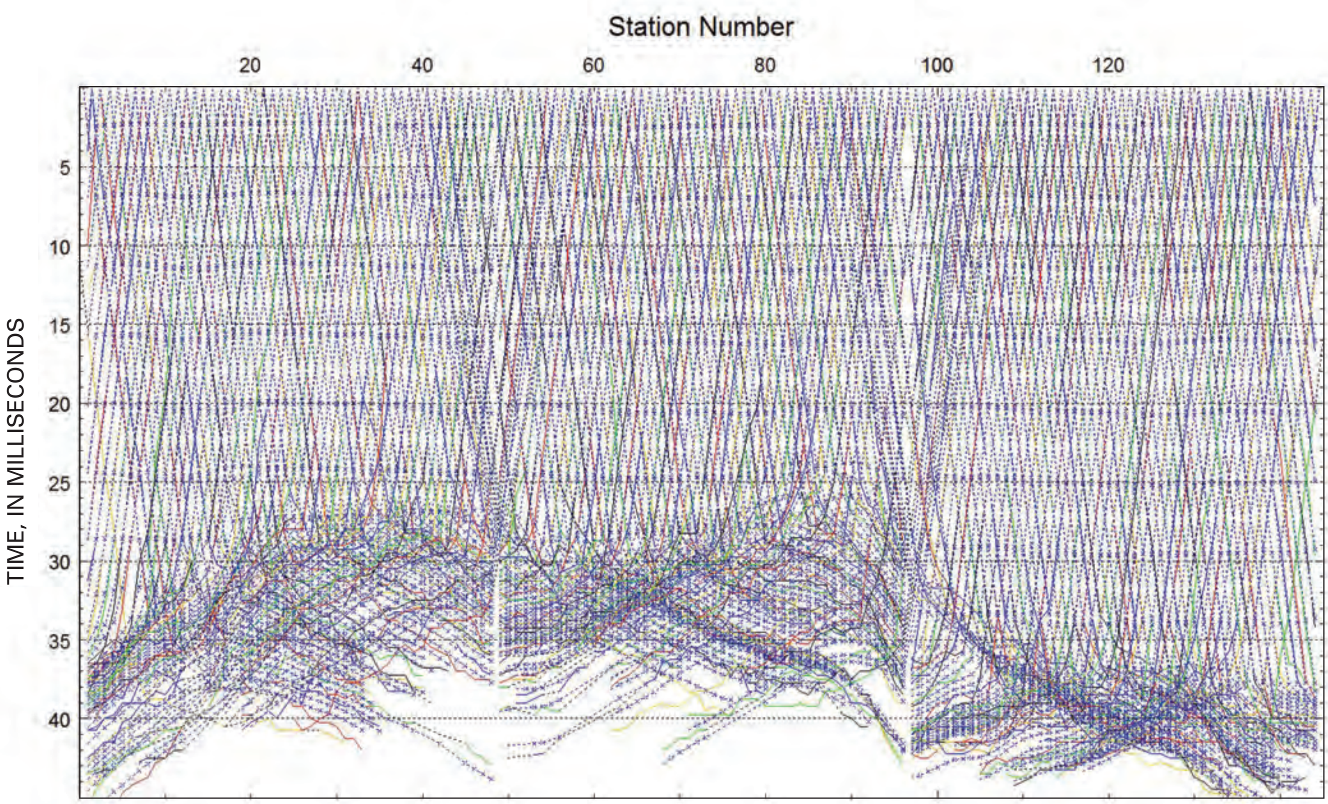

Seismic Line 6

Station spacing = 1.5 m

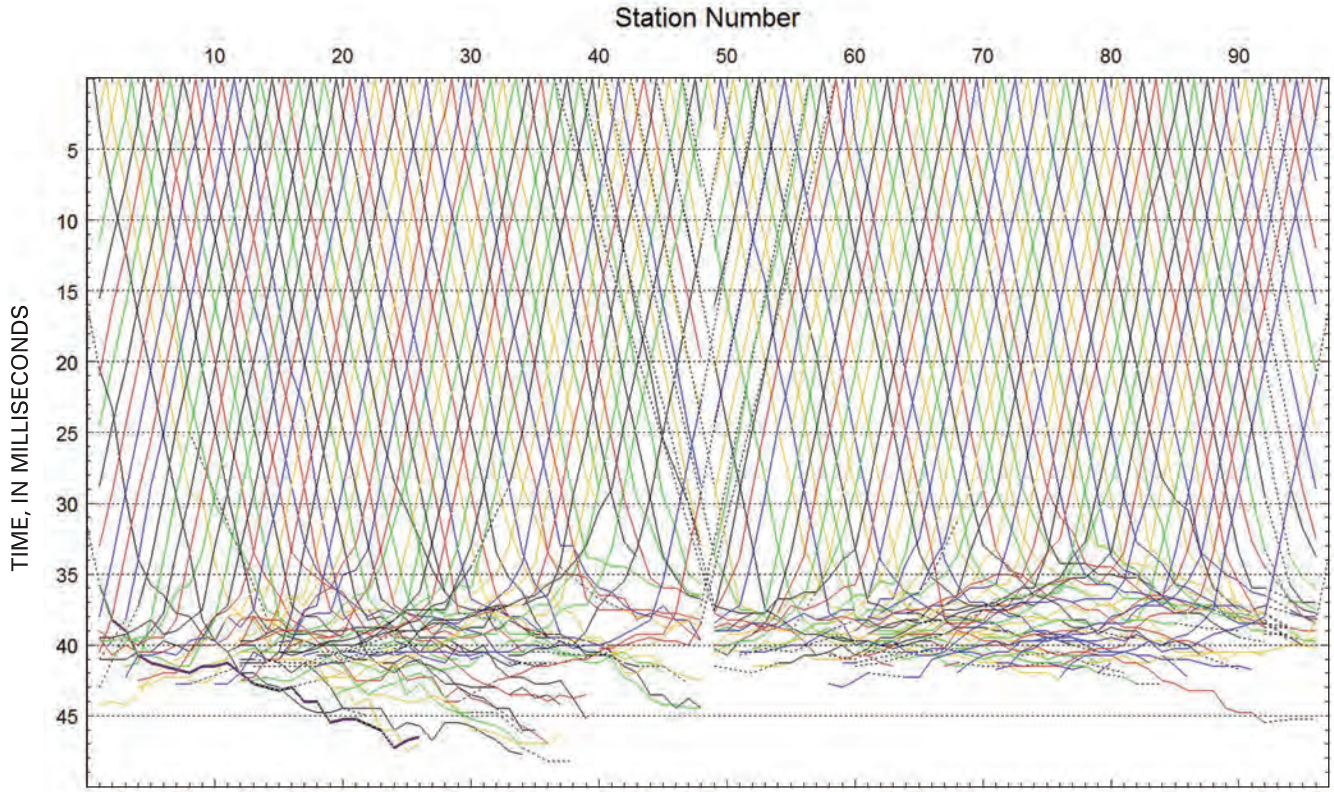

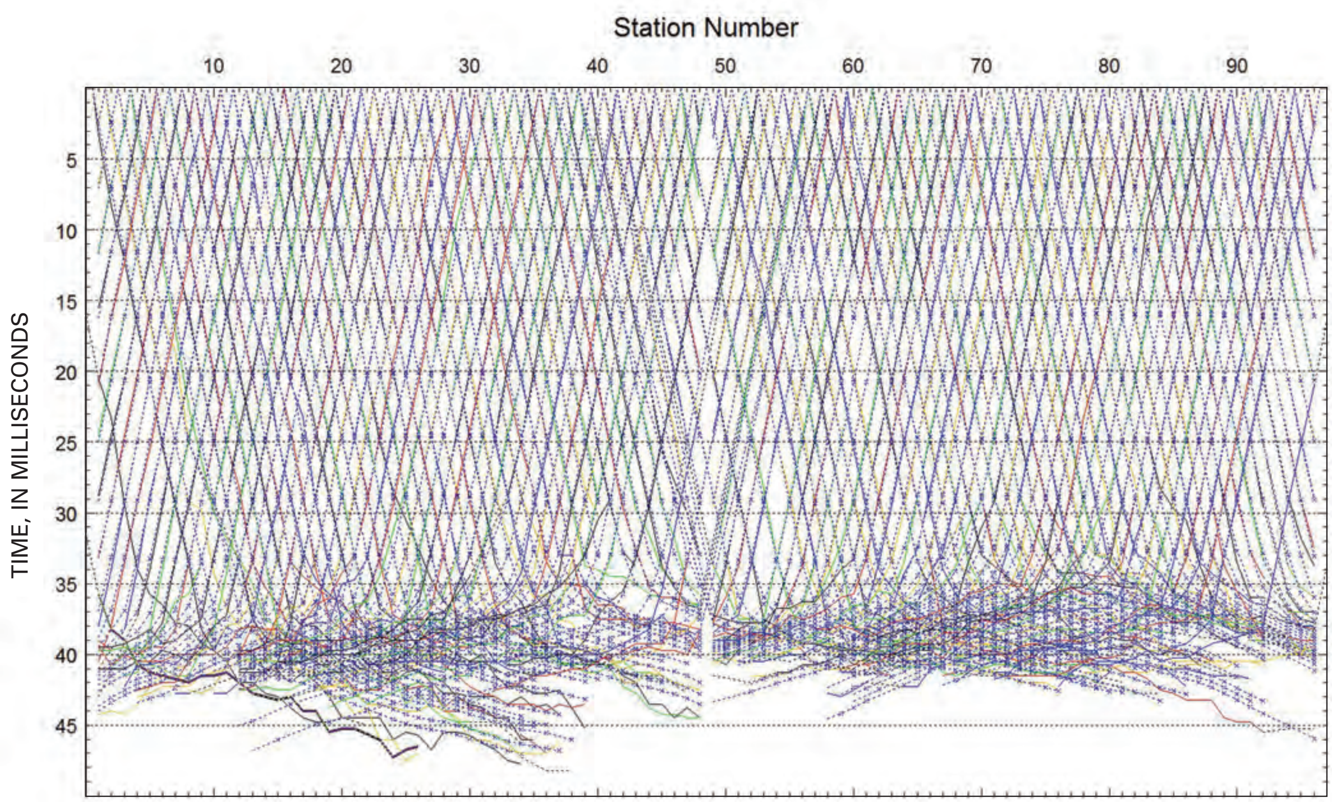

Publishing support provided by:
Denver Publishing Service Center, Denver, Colorado
Manuscript approved for publication October 29, 2008
Edited by Melanie Parker
Graphics and layout by Joy Monson

For more information concerning this publication, contact:
Team Chief Scientist, USGS Crustal Imaging and Characterization
Box 25046, Mail Stop 964
Denver, CO 80225
(303) 236-1312

Or visit the Crustal Imaging and Characterization Team Web site at:
http://crustal.usgs.gov/

This publication is available online at:
http://pubs.usgs.gov/sir/2008/5212/

USGS

Burton and others—**Integrated Geophysical Investigation of Preferential Flow Paths near Eureka, Missouri, May 2006**—USGS/SIR 2008–5212